

Research Article

Lack of mitochondrial NADP(H)-transhydrogenase expression in macrophages exacerbates atherosclerosis in hypercholesterolemic mice

Alessandro G. Salerno^{1,*}, Thiago Rentz^{1,*}, Gabriel G. Dorighello^{1,*}, Ana Carolina Marques², Estela Lorza-Gil¹, Amarylis C. B. A. Wanschel¹, Audrey de Moraes², Anibal E. Vercesi² and  Helena C. F. Oliveira¹

¹Department of Structural and Functional Biology, Institute of Biology, State University of Campinas, Campinas, SP, Brazil; ²Department of Clinical Pathology, Faculty of Medical Sciences, State University of Campinas, Campinas, SP, Brazil

Correspondence: Helena C. F. Oliveira (ho98@unicamp.br)

The atherosclerosis prone LDL receptor knockout mice ($Ldlr^{-/-}$, C57BL/6J background) carry a deletion of the NADP(H)-transhydrogenase gene (*Nnt*) encoding the mitochondrial enzyme that catalyzes NADPH synthesis. Here we hypothesize that both increased NADPH consumption (due to increased steroidogenesis) and decreased NADPH generation (due to *Nnt* deficiency) in $Ldlr^{-/-}$ mice contribute to establish a macrophage oxidative stress and increase atherosclerosis development. Thus, we compared peritoneal macrophages and liver mitochondria from three C57BL/6J mice lines: *Ldlr* and *Nnt* double mutant, single *Nnt* mutant and wild-type. We found increased oxidants production in both mitochondria and macrophages according to a gradient: double mutant > single mutant > wild-type. We also observed a parallel up-regulation of mitochondrial biogenesis (PGC1a, TFAM and respiratory complexes levels) and inflammatory (iNOS, IL6 and IL1b) markers in single and double mutant macrophages. When exposed to modified LDL, the single and double mutant cells exhibited significant increases in lipid accumulation leading to foam cell formation, the hallmark of atherosclerosis. *Nnt* deficiency cells showed up-regulation of CD36 and down-regulation of ABCA1 transporters what may explain lipid accumulation in macrophages. Finally, *Nnt* wild-type bone marrow transplantation into $LDLr^{-/-}$ mice resulted in reduced diet-induced atherosclerosis. Therefore, *Nnt* plays a critical role in the maintenance of macrophage redox, inflammatory and cholesterol homeostasis, which is relevant for delaying the atherogenesis process.

Introduction

The oxidative modification hypothesis of atherogenesis proposes that low-density lipoprotein (LDL) is a major target of oxidation in the arterial subendothelial space and is involved in both the initiation and progression of atherosclerosis [1,2]. Oxidized LDL induces endothelium activation and recruitment of circulating monocyte, which differentiate into macrophages that continuously take up the modified LDL turning into cholesterol engorged foam cells. Although many cell types, including endothelial cells, monocytes, dendritic cells (DCs), lymphocytes and smooth muscle cells, contribute to the formation of atherosclerotic plaques, macrophage-derived foam cells are considered the hallmark of early atherosclerosis [3]. There is strong support for the occurrence of a vascular wall oxidative stress during atherogenesis, however the multiple and cell type-specific mechanisms that drive *in vivo* oxidation have not been completely characterized yet [4].

Oxidative phosphorylation in mitochondria of all eukaryotic cells produces regulated levels of superoxide radicals that can be converted to hydrogen peroxide and ultimately to water by an efficient antioxidant enzyme system. While this is part of signaling and adaptive responses under physiological conditions [5], excessive mitochondria derived reactive oxygen species have been correlated with a

*These authors contributed equally to this work.

Received: 26 July 2019
 Revised: 4 December 2019
 Accepted: 4 December 2019

Accepted Manuscript online:
 5 December 2019
 Version of Record published:
 20 December 2019

number of diseases, including atherosclerosis [6–12]. Mitochondrial oxidants production is commonly promoted by high microenvironment calcium concentrations and causes mitochondrial permeability transition (MPT). MPT, a process first described by Hunter et al. [13], is a condition characterized by the opening of a nonspecific proteinaceous pore that leads to mitochondrial dysfunction and cell death [14]. However, mitochondria also have a high antioxidant capacity that is largely dependent on the NADPH pool. Hydrogen peroxide is removed by catalase in the cytosol and by glutathione/thioredoxin peroxidases, at the expense of glutathione (GSH) and thioredoxin (Trx) in the mitochondrial matrix. The oxidized form of glutathione and Trx are then reduced back by glutathione/thioredoxin reductases, respectively, at the expense of NADPH as reducing power. Mitochondrial NADPH is, in turn, regenerated mainly by the mitochondria membrane potential-dependent NAD(P)H transhydrogenase (Nnt). This enzyme is located in the inner mitochondrial membrane, where it functions as a homodimeric redox-dependent proton pump that uses the proton gradient across the inner mitochondrial membrane to catalyze the generation of NADPH and NAD⁺ from NADP⁺ and NADH in the mitochondrial matrix [15,16]. Hence, Nnt is coupled to mitochondrial metabolism, which is, in turn, coupled to NADPH generation and oxidants detoxification [15–18].

The spontaneous genetic deletion of Nnt gene discovered in C57BL/6J mice in 2005 [19] has been considered a plausible explanation for metabolic phenotypes such as glucose intolerance and defective insulin secretion in these mice [19–23]. The absence of Nnt is thought to elevate mitochondrial H₂O₂ production within the beta cell in response to glucose metabolism, thereby lowering the ATP:ADP ratio, delaying closure of the K_{ATP} channel and ultimately impairing insulin secretion [24]. Recently, Leskov et al. [25] described that the absence of Nnt results in the development of hypertension in mice. In addition, Nnt is highly expressed in bone marrow and other immune response-related tissues, such as spleen, lung, liver and macrophages, suggesting a function in immunity and inflammatory responses [26].

We have previously shown that liver, heart, brain and spleen mitochondria from the hypercholesterolemic atherosclerosis prone LDL receptor knockout (Ldlr^{-/-}) mice generate more oxidants than controls, and that mitochondrial oxidants production rates correlate with the size of aortic atherosclerosis in this model [6,7,27]. We also showed in Ldlr^{-/-} mice higher liver steroidogenesis and lipid secretion rates, in order to compensate for the lack of LDL cholesterol uptake. We proposed that the increased steroidogenesis in Ldlr^{-/-} mice deplete the reducing equivalents from NADPH pool generating a mitochondria and cell redox imbalance [27]. In addition, Ldlr^{-/-} mice on the C57BL/6J background carry the Nnt gene mutation. Therefore, here we tested the hypothesis that both increased NADPH consumption (due to increased steroidogenesis) and decreased NADPH generation (due to Nnt deficiency) in Ldlr^{-/-} mice contribute to establish a cell oxidative stress in their tissues increasing oxidative stress and the susceptibility to atherosclerosis. We focus this study on the key inflammatory cell type for atherosclerosis, the macrophages and the process of foam cell formation, as well as, on the *in vivo* process of atherosclerosis development.

Materials and methods

Mice

C57BL/6JUnib, C57BL/6J and LDL receptor knockout (Ldlr^{-/-} on the C57BL/6J background) mice were provided by the State University of Campinas Multidisciplinary Center for Biological Research in Laboratory Animals (CEMIB/Unicamp, Campinas, Brazil). All three C57BL/6J colonies were established with founders from The Jackson Laboratory. Ldlr^{-/-} and C57BL/6J controls were purchased from The Jackson Laboratory (Bar Harbor, ME, U.S.A.) in 2009, while the C57BL/6JUnib colony was supplied by the Zentralinstitut für Versuchstierzucht (ZfV) (Hannover, Germany) in 1987, which had previously been obtained from The Jackson Laboratory. C57BL/6J and C57BL/6JUnib mice are homozygous for mutated and wild-type Nnt alleles, respectively. This mutation in C57BL/6J comprises a 17 814-bp deletion in the Nnt gene that arose spontaneously and was named *NntC57BL/6J* in the MGI data bank (<http://www.informatics.jax.org/>). All experimental protocols were approved by the University's Committee for Ethics in Animal Experimentation (CEUA/UNICAMP, protocols #3337-1 and #3814-1) and all experiments were performed in accordance with the national Brazilian guideline number 13 for 'Control in Animal Experiments', published on September 13th, 2013 (code 00012013092600005, available at <http://portal.in.gov.br/verificacao-autenticidade/>). All animal work was done in the Laboratory of Lipid Metabolism, Dept of Structural and Functional Biology, Institute of Biology, State University of Campinas. Mice were kept under standard laboratory conditions (at 20–22°C and a 12 h/12 h light/dark cycle) in the local (conventional) animal facility, in individually ventilated cages (3–5 mice/cage),

with free access to filtered tap water and regular rodent AIN93-M diet (standard laboratory rodent chow diet, Nuvital CR1, Colombo, PR, Brazil). After PCR genotyping, C57BL/6JUnib, C57BL/6J and *Ldlr*^{-/-} mice were named, respectively, *Nnt*^W (controls), *Nnt*^{Mut} (single *Nnt* mutant) and *Ldlr*^{Mut}*Nnt*^{Mut} (*Ldlr* and *Nnt* double mutant). Male mice (12–16 weeks of age) from each genotype were used to obtain peritoneal macrophages ($n = 6$ /group). Male mice (10–12 weeks of age) from each genotype were used to obtain liver and heart mitochondria ($n = 10$ –12/group). Two additional groups of *Ldlr*^{Mut}*Nnt*^{Mut} mice were randomly assigned to be recipients ($n = 6$ /group) of bone marrow transplants from *Nnt*^{Mut} or *Nnt*^W donor mice ($n = 6$ /group). For primary macrophages and isolated mitochondria experiments, mice were anesthetized by isoflurane inhalation and killed by cervical dislocation. For terminal experiments with transplanted mice, anesthesia was ketamine and xylazine (50 and 10 mg/kg), *ip*, followed by exsanguination through the retro-orbital plexus. All animal experiments were performed between 8:00 and 11:00 pm. Non-fasting plasma cholesterol and triglycerides were measured using standard commercial kits (Roche Diagnostics GmbH, Mannheim, Germany) according to the manufacturer's instructions.

PCR genotyping protocol for identification of the *Nnt* mutation

DNA was extracted from mice tails by proteinase K digestion [28]. Briefly, 2 mm of mouse tails were incubated in 50 μ l of 1 \times Gitschier buffer (67 mM Tris-HCl pH 8.8, 16.6 mM (NH₄)₂SO₂, 6.5 mM MgCl₂) with 1% β -mercaptoethanol, and 0.5% Triton X-100 at 95°C for 5 min. Proteinase K was then added to a final concentration of 1 mg/ml. Tails were digested at 55°C for 2 h and then incubated at 95°C for 10–20 min to heat denature the proteinase K. An amount of 1 μ l of tail digests was used for subsequent PCR amplification. *Nnt*^W, *Nnt*^{Mut}, *Ldlr*^{Mut}*Nnt*^{Mut} mice groups were genotyped using a three-primer, two-allele PCR assay to discriminate between the *Nnt* wild-type allele and the mutant allele lacking *Nnt* exons 7–11 [29]. The primer sequences were (all 5'–3'): *Nnt*-COM (GTAGGGCCAACCTGTTTCTGCATGA); *Nnt*-WT (GGGCATAGGAAGCAAATACCAAGTTG); *Nnt*-MUT (GTGGAATCCGCTGAGAGAACTCTT). The 'COM' primer participates in amplification of the all three groups, while the 'WT' and 'MUT' primers are specific to the wild-type and *Nnt*^{Mut} (mutant) alleles, respectively. Amplification conditions used were initial cycle of 95°C, 5 min; then 35 cycles of 95°C, 45 s, 58°C, 30 s, 72°C, 45 s; followed by a final extension of 5 min at 72°C. Products of PCR amplification were 579 bp for the wild-type allele and 743 bp for the mutant allele. The products of PCR reactions were subjected to electrophoresis in a 2% agarose gel, staining with ethidium bromide, and visualization on a UV light box using a commercial imaging system (Bio-Rad ChemiDoc™ XRS Gel Documentation system).

Peritoneal macrophages isolation

Peritoneal macrophages from adult *Nnt*^W, *Nnt*^{Mut} and *Ldlr*^{Mut}*Nnt*^{Mut} mice ($n = 6$ /group) were isolated as previously described [30]. Mice were injected intraperitoneally with 1 ml of 3% (wt/vol) thioglycolate to elicit sterile peritonitis with macrophage numbers peaking on day 4. Cells were collected by lavage and maintained in culture as an adherent monolayer in medium containing DMEM, 10% FBS, and 20% L929-cell conditioned medium during 48 h before analyses. All cells were cultured in a humidified incubator at 37°C and 5% CO₂.

Western-blot analysis

The peritoneal macrophages were homogenized in RIPA lysis buffer containing 1% protease inhibitor cocktail. The protein content from collected cells was analyzed by electrophoresis on an 8–10% polyacrylamide gel containing sodium dodecyl sulfate and then transferred to nitrocellulose/PVDF membrane. Western-blot analyses were carried out according to standard protocols with antibodies raised against *Ldlr* (10240; Cayman Chem. Co.), *Nnt* (bs5097R; Bioss), HMG-CoA red (abs229; Millipore), SOD2 (ab13533-50; abcam), ABCA1 (ab18180; abcam), ABCG1 (ab36969-100; abcam), SRB1 (NB400-113; Novus Biologicals), SREBP-1 (ab3259; abcam), PGC-1 α (sc-13067; Santa Cruz Biotech.), mtTFA (sc-28200; Santa Cruz Biotech.), OXPHOS (ab110413; abcam), CD36 (ab17044; abcam), SRA (ab36998; abcam) and β -actin (AM4302; Thermo Scientific), α -tubulin (sc-8035; Santa Cruz Biotech.) and HSP90 (#4874; Cell Signaling Technology) were used as internal controls. Immuno-detection was performed using an enhanced chemiluminescence detection kit. Band intensities were quantified using ImageJ software (NIH-ImageJ, U.S.A.).

Real time PCR

Peritoneal macrophage mRNA was extracted by RNeasy kit (#7400, Qiagen), then 1 μ g of purified mRNA was used to synthesize the cDNA (High-Capacity cDNA reverse transcription kit, Applied Biosystems, Foster City,

CA). Relative quantification was performed using the Step-one real-time PCR system (Applied Biosystems). The primers were designed and tested against the *Mus musculus* genome (GenBank). The relative quantities of the target transcripts were calculated from duplicate samples ($\Delta\Delta CT$), the data were normalized against the endogenous control HPRT (hypoxanthine phosphoribosyl transferase). The primer sequences were as follows: mouse **Ldlr**, 5'-AGGCTGTGGGCTCCATAGG-3' and 5'-TGCGGTCCAGGTCATCT-3'; **HMGCR**, 5'-TTCTC GTGAAAGCCGTGAGG-3' and 5'-TGAGCGTGAACAAGGACCAA-3'; **SOD2**, 5'-ACTGAAGTTCAATGGTG GTGGGG-3' and 5'-GCTTGATAGCCTCCAGCAAC-3'; **HPRT** (hypoxanthine phosphoribosyltransferase), 5'-GGTAAAGCAGTACAGCCCCA-3' and 5'-TCCAACACTTCGAGAGGTCC-3'; **CD36**, 5'-GGAAGTGTGGG CTCATTGC-3' and 5'-CATGAGAATGCCTCCAAACAC-3'; **ABCA1**, 5'-CGTTTCCGGGAAGTGTCCCTA-3' and 5'-GCTAGAGATGACAAGGAGGATGGA-3'. The expression of inflammatory markers were determined using the following primers sequences: **TNF α** , 5'-CCCTCCTGGCCAACGGCATG-3' and 5'-TCGGGGCAGC CTTGTCCCTT-3'; **iNOS**, 5'-GTTCTCAGCCCAACAATACAAGA-3' and 5'-GTGGACGGGTTCGATGTCAC-3'; **IL-6**, 5'-CACGGCCTTCCCTACTTCAC-3' and 5'-GGTCTGTTGGGAGTGGTATC-3'; **IL-1b**, 5'-CCTTCCAGG ATGAGGACATGA-3' and 5'-TGAGTCACAGAGGATGGGCTC-3'; and **36B4** (acidic ribosomal phosphoprotein), 5'-GAGGAATCAGATGAGGATATGGGA-3' and 5'-AAGCAGGCTGACTTGGTTGC3'.

Production of H₂O₂ by peritoneal macrophages

To assay the production of H₂O₂, 0.5×10^5 peritoneal macrophage cells were incubated in 96-well cell culture plates. On the day of the experiment, cells were incubated in a mixture contained 50 μ M Amplex Red reagent (Invitrogen) and 0.1 U/ml horseradish peroxidase in Krebs-Ringer phosphate (145 mM NaCl, 5.7 mM sodium phosphate, 4.86 mM KCl, 0.54 mM CaCl₂, 1.22 mM MgSO₄, 5.5 mM glucose, pH 7.35). This assay was conducted in the presence and absence of catalase (1000 U/ml). Fluorescence was monitored over time with a temperature-controlled SpectraMax M3 Microplate Reader (Molecular Devices LLC) using excitation and emission wavelengths of 560 and 590 nm, respectively. Results were expressed as μ M of H₂O₂/60 min/ 0.5×10^5 peritoneal macrophage cells using the standard curve established in each assay with known molar concentrations of H₂O₂.

Flow cytometry cell superoxide production measurement

The superoxide indicator dihydroethidium (DHE) exhibits blue-fluorescence in the cytosol until oxidized, where it intercalates within the cell's DNA, staining its nucleus a bright fluorescent red. DHE (Molecular Probes, ThermoFisher) was added to the cells (1×10^6 cells/ml of peritoneal macrophage) at final concentration of 5 μ M in culture media and incubated at 37°C for 30 min. Each aliquot was analyzed using a FACSCalibur flow cytometer (BD Biosciences, San Jose, CA, U.S.A.) equipped with an argon laser and CellQuest software (version 4.1) with excitation at 488 nm and emission at 620 nm. A minimum of 10 000 events was collected. Results are presented as relative probe fluorescence intensity expressed as fold changes.

Measurement of mitochondrial superoxide production in cultured macrophages

Peritoneal macrophages were seed on eight wells LabTek slides (Thermo Scientific) using a DMEM 10% FBS, and 20% L929-cell conditioned medium. On the day of the experiment, cells were pre-incubated with 5 μ M of the mitochondrial superoxide indicator MitoSOX (Molecular Probes, Invitrogen) at 37°C for 30 min. For live-cell imaging, cells were then rinsed in warm culture medium and stained with Mitotracker Green (Molecular Probes, Invitrogen) (100 nM) at 37°C for 15 min, followed by three washes with a warm medium. Nuclei were counterstained with DAPI for 10 min. Cells were mounted onto glass slides with Mounting Medium Vectashield (Vector Laboratories). Images of cells were acquired using a Leica LSM 780 confocal microscope with 63 \times objective, followed by measurement of the average cell area of at least 10 cells per field using ImageJ software.

GSH and GSSG measurement

Reduced glutathione (GSH) and oxidized glutathione (GSSG) measurement methods were adapted from Hissin and Hilf [31] using a reaction between GSH and O-phthalaldehyde (OPT) 1 mg/ml in sodium phosphate buffer 100 mM, EGTA 6 mM, pH 7.4, and between GSSG and OPT in 1 M NaOH, pH 12 in the presence of N-ethylmaleimide (NEM) 2 mM to avoid GSH interference in GSSG quantification. Samples were prepared by

protein precipitation (200 μ g) with RIPA lysis buffer containing 1% protease inhibitor cocktail and measured using a SpectraMax M3 Microplate Reader (Molecular Devices LLC) by excitation and emission wavelengths of 350 nm and 420 nm, respectively.

Modified-LDL induced foam cell formation

DiI-acetylated-LDL was purchased from Biomedical Technologies. DiI is a lipophilic stain that is orange-red fluorescent. Mouse peritoneal macrophages were seeded onto glass coverslips in macrophage growth medium. Cells were washed once in 1 \times PBS and incubated in fresh media containing DiI-Ac-LDL (30 μ g cholesterol/ml) for 2 h at 37°C. At the end of the incubation period, cells were washed and 1 ml of RPMI 10% FBS added for 15 min at 37°C to allow the internalization. Nuclei were counterstained with DAPI for 10 min. Finally, cells were mounted onto glass slides with mounting medium (Vector Lab). Images of cells were acquired using a Leica Upright LSM780-NLO confocal microscope with 20 \times and 63 \times Plan objectives. Additional experiments of foam cell induction were performed using oxidized-LDL (60 μ g/ml, Alfa Aesar, MA, U.S.A.) incubated with mouse peritoneal macrophages during 6 h in medium without FBS. Cells were then washed with PBS, incubated with catalase 20 U during 15 min at 37°C in order to eliminate any peroxides present in the samples [32,33] and had the cholesterol content quantified using the Amplex Red kit according to the manufacturer's instructions (Thermo Fisher Scientific). The cholesterol uptake was calculated by the difference between total cell cholesterol content in incubations with oxLDL minus incubation without oxLDL.

Mitochondria isolation, oxidants production, swelling and membrane potential assays

Mitochondria were isolated from liver and hearts of mice by differential centrifugation [34] with slightly modifications as described previously [35]. Assays were conducted in a standard reaction medium (28°C) containing 125 mM sucrose, 10 mM Hepes, 2 mM K_2HPO_4 , 65 mM KCl, 1 mM $MgCl_2$ and 14.2 μ M Ca^{2+} (pH 7.2). A pool of 5 mM NAD-linked substrates containing glutamate, malate, α -ketoglutarate and pyruvate was used as a substrate for the respiratory chain. The global net reactive oxygen species production by mitochondria (0.5 mg/ml) was monitored using the membrane-permeable fluorescent dye 2',7'-dichlorodihydrofluorescein diacetate (H_2 -DCFDA, 1 μ M) as previously described [27]. Fluorescence was determined at 488 nm for excitation and 525 nm for emission. A calibration curve was obtained with known concentrations of dichlorofluorescein (DCF), the product of H_2 -DCF-DA oxidation. H_2O_2 release from isolated mitochondria (0.5 mg/ml) was monitored by measuring the conversion of Amplex Red (10 μ M) to highly fluorescent resorufin in the presence of added horseradish peroxidase (1 U/ml). Resorufin fluorescence was measured at 563 nm for excitation and 587 nm for emission. Mitochondrial swelling was determined as the decrease in the turbidity of the mitochondrial suspension measured at 520 nm in a Hitachi U-3000 spectrophotometer. The mitochondrial transmembrane electrical potential was determined by fluorescence changes of safranin O (5 μ M) in a spectro-fluorometer (Hitachi F/4500) operating at 495 nm excitation and 586 nm emission wavelengths [36].

Bone marrow transplantation and diet-induced atherosclerosis

Male $Ldlr^{-/-}$ mice (36 weeks of age) were exposed to a single 8.0-Gy total-body irradiation using a cobalt-60 source (Theratron-780 model; MDS Nordion). Within 24 h after irradiation, mice randomly assigned to receive a tail vein injection of 5.0×10^6 bone marrow cells freshly collected from male donor mice lines: Nnt^{Mut} and Nnt^W . The cells were aseptically harvested by flushing donor femurs with Dulbecco's PBS containing 2% fetal bovine serum. Samples were filtered through a 40 μ m nylon mesh and centrifuged at room temperature for 10 min at 1000 rpm. Cells were resuspended in Dulbecco's PBS at a concentration of 5.0×10^6 viable nucleated cells in 200 μ l for each mouse. Irradiated mice transplanted with this suspension were housed in autoclaved cages and treated with antibiotics (0.2 mg trimethoprim and 1.0 mg/ml sulfamethoxazole) in the drinking water given for 4 days before and 7 days after the irradiation. Then, transplanted mice received a western type diet containing (g%): protein 20, carbohydrate 50, fat 21 (mostly saturated) and cholesterol 0.21 (Detailed composition in Supplementary Table S1) (Prag Soluções, Jaú, SP, Brazil) for the next 8 weeks. The mineral and vitamin mixtures were as AIN-93M recommended for rodents by the American Institute of Nutrition (detailed composition and ingredients are provided in the Supplemental Data). The hearts of anesthetized mice (xylazine/ketamine, 10 and 50 mg/Kg respectively) were perfused *in situ* with phosphate-buffered saline (PBS) followed by 4% PBS-buffered formaldehyde. Hearts were then excised and embedded in Tissue-Tek® OCT

compound (Sakura Inc., Torrance, CA, U.S.A.) and frozen at -80°C . The tip of the heart (ventricle) was removed with a surgical knife and serial sections of $60\ \mu\text{m}$ were cut and discarded until the visualization of the aortic sinus leaflets. Then, sections were reduced to $10\ \mu\text{m}$ thickness and cut along a $470\ \mu\text{m}$ aorta length. Sections were stained with Oil Red O as previously described [6]. The areas of the lesions were calculated as the sum of lipid stained lesions in six sections per mouse (one section every $80\ \mu\text{m}$ along the aorta length). The lipid stained lesions were quantified using the Image J (1.45 h) software. The same procedure of cryo-sectioning was employed in additional hearts for immunofluorescence staining for CD68 (macrophages) and nitrotyrosine (indicator of cell oxidative damage and inflammation mediated by reactive nitrogen species such as peroxynitrite anion). Sections were blocked with 10% bovine serum albumin (BSA) and then incubated for 2 h at 22°C (CD68) or overnight (nitrotyrosine) at 4°C with the following primary antibodies: CD68 (1 : 200; Bio-Rad) or biotinylated nitrotyrosine (3-NT) (1 : 100; Cayman Chemical). Sections were washed and incubated with fluorescently-labeled secondary antibody Alexa Fluor-conjugated (Invitrogen). Nuclei were counterstained with DAPI for 10 min. Sections were mounted with Vectashield medium and microscopic images of aortic lesions (objective lenses $10\times$) were digitalized, and morphometric measurements were calculated as described for Oil red O. Image J software (NIH-ImageJ, U.S.A.) was used for all the quantifications. All slides were read without group identification (blindly).

Statistical analysis

Data are presented as mean \pm the standard error (SE), n (number of animals) is stated in the figure legends, and the statistical differences were evaluated using one way ANOVA followed by Tukey posttest for multiple comparisons or Student's t -test for two means comparisons. Animal sample size (n) for each experiment was chosen based on literature documentation of the similar studies. Significance was accepted at the level of $P < 0.05$.

Results

We first confirmed that control wild-type (Nnt^{W}) mice were homozygous for the wild-type full-length *Nnt* allele and that *Nnt* single mutant (Nnt^{Mut}) and LDLr + *Nnt* double mutant ($\text{Ldlr}^{\text{Mut}}\text{Nnt}^{\text{Mut}}$) mice were homozygous for the mutated *Nnt* allele. Using genomic DNA from the tail tip, PCR was performed to amplify a fragment of either the wild-type (579 bp) or the mutated (743 bp) *Nnt* allele (Figure 1A). Next, we validated peritoneal macrophages from the three groups regarding specific proteins of interest (Figure 1B). Protein expression of *Nnt* was detected only in the control macrophages (Nnt^{W}). *Ldlr* protein expression confirmed lack of western blot band in $\text{Ldlr}^{\text{Mut}}\text{Nnt}^{\text{Mut}}$ group. As expected, HMG-CoA reductase, which encodes the rate-limiting enzyme in the cholesterol synthesis pathway, is increased in the $\text{Ldlr}^{\text{Mut}}\text{Nnt}^{\text{Mut}}$ group, and similarly expressed in Nnt^{W} and Nnt^{Mut} mice. Finally, we found that the protein expression of the mitochondrial manganese-dependent superoxide dismutase (SOD2) is increased in macrophages of $\text{Ldlr}^{\text{Mut}}\text{Nnt}^{\text{Mut}}$ compared with Nnt^{W} mice (Figure 1B). This antioxidant enzyme is up-regulated in conditions of high superoxide production. The *Ldlr*, HMGCoA reductase and SOD2 mRNA expression levels in peritoneal macrophages from the three groups (Figure 1C) are in accordance with their respective protein levels (Figure 1B).

To investigate the role of *Nnt* and *Ldlr* on the cell oxidants production, macrophages from the three groups of mice were incubated with probes sensitive to various reactive oxygen. H_2O_2 production rates were measured using the Amplex Red/horseradish peroxidase assay (Figure 2A). $\text{Ldlr}^{\text{Mut}}\text{Nnt}^{\text{Mut}}$ mice peritoneal macrophages presented marked higher rates ($\sim 70\%$) of H_2O_2 production than those of Nnt^{Mut} and Nnt^{W} mice cells. This result is likely related to the increased SOD2 protein expression in the $\text{Ldlr}^{\text{Mut}}\text{Nnt}^{\text{Mut}}$ group, as an attempt to protect cell against high superoxide production. A slight but non-significant increase in H_2O_2 release rate (15%) was observed in Nnt^{Mut} compared with Nnt^{W} cells (Figure 2A).

To include superoxide in the oxidants production rates, the superoxide sensitive DHE probe was employed. The method is sensitive, but its main drawback is that the total fluorescence of DHE is a sum of different fluorescent products. While 2-hydroxyethidium is generated specifically by superoxide oxidation of DHE, ethidium is associated mainly with pathways involving hydrogen peroxide and metal-based oxidizing systems, including heme proteins and peroxidases. In addition, the ethidium product can represent the decay of 2-hydroxyethidium and potentially of other fluorescent intermediate products [37]. Thus, DHE derived fluorescence reflects the total cell redox state rather than the production of a specific intermediate. Here, macrophages were incubated with DHE in the presence and absence of the NADPH oxidase inhibitor (DPI). Both *Nnt* mutant cells, Nnt^{Mut} and $\text{Ldlr}^{\text{Mut}}\text{Nnt}^{\text{Mut}}$, showed significantly increased DHE derived fluorescence, 22 and

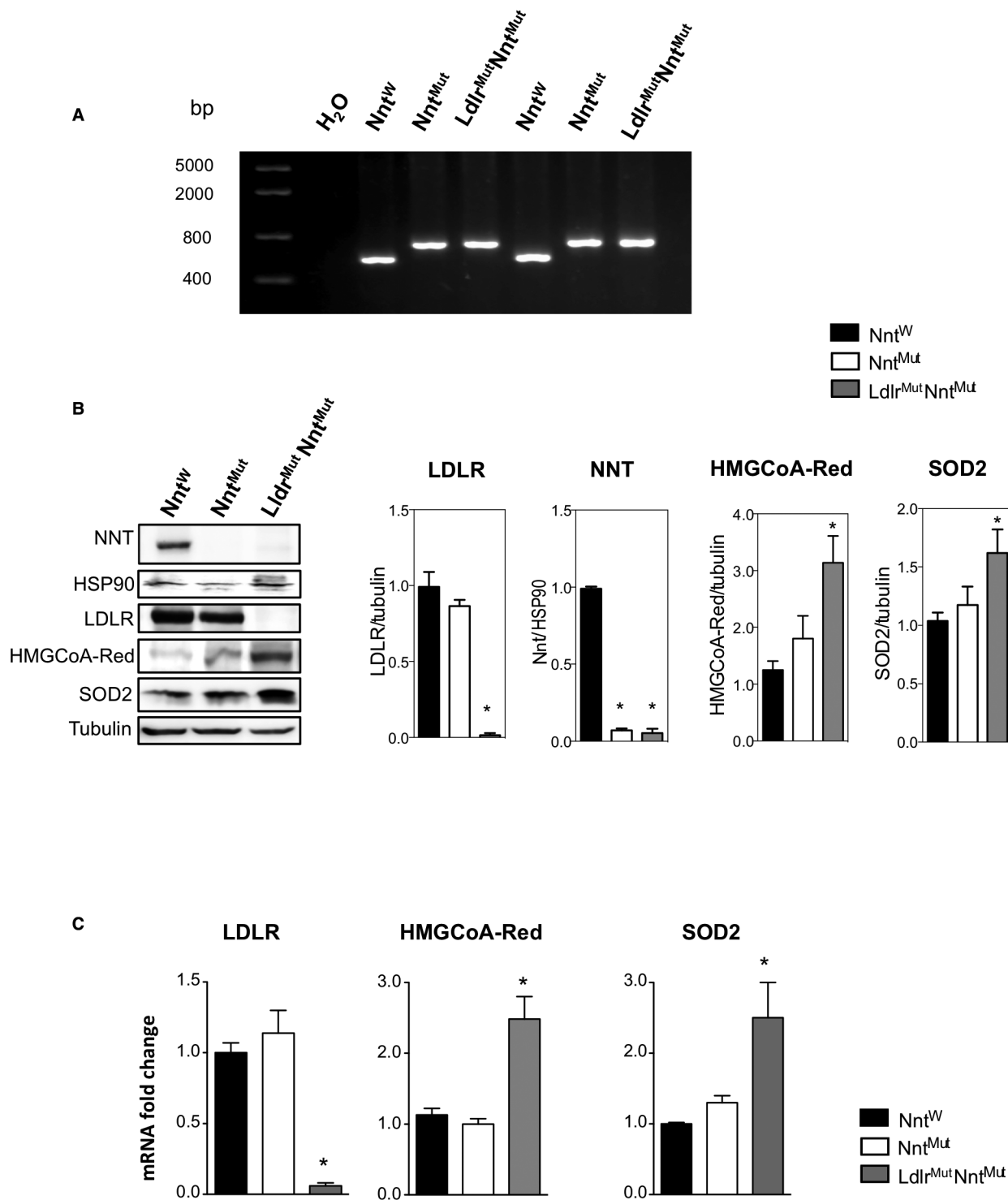
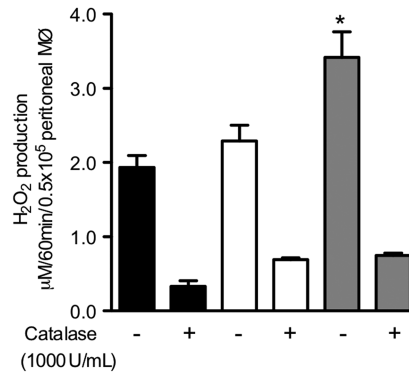


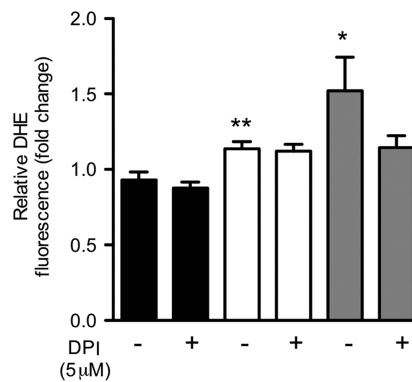
Figure 1. Characterization of macrophages of the three C57BL/6J mice lines: Nnt^W (control), Nnt^{Mut} (single mutant) and Ldlr^{Mut}Nnt^{Mut} (double mutant) mice.

(A) Mice Nnt genotyping — genomic DNA PCR amplification products of the mutated (743 bp) and wild-type (579 bp) Nnt gene (B) Protein expression levels of the LDL receptor (LDLR), NADP-transhydrogenase (Nnt), hydroxyl methyl glutaryl coenzyme A reductase (HMGCoA-Red) and superoxide dismutase isoform 2 (SOD2) (C) and respective mRNA expression levels normalized by HPRT. Mean ± SE ($n = 5$), * $P < 0.05$ vs Nnt^W (control), one-way ANOVA with Tukey's posttest.

A H₂O₂



B DHE



C GSH/GSSG

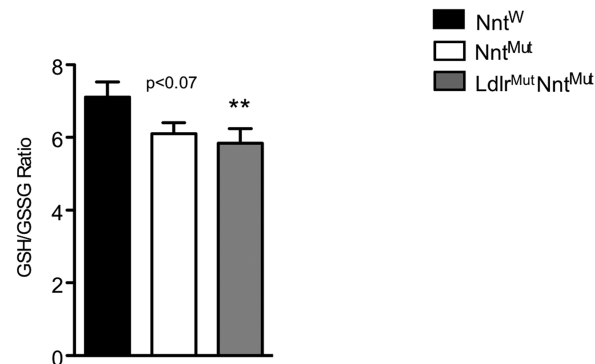


Figure 2. Reactive oxygen species production is increased and GSH:GSSG ratio is decreased in Nnt and Ldlr mutant macrophages.

(A) H₂O₂ production assayed using Amplex Red and (B) dihydroethidium (DHE) derived fluorescent oxidized products. (C) Ratio of reduced to oxidized glutathione (GSH:GSSG). Mean ± SE, *n* = 4–6. * *P* < 0.05 vs Nnt^W (control), one-way ANOVA with Tukey's posttest. ** *P* < 0.05 vs Nnt^W (control), Student's *t*-test.

67%, respectively, compared with the control Nnt^W (Figure 2B). Besides, Ldlr^{Mut}Nnt^{Mut} double mutant macrophages showed increased oxidized DHE signal compared with the Nnt^{Mut} single mutant cells. Therefore, we observed significant differences in oxidants production and oxidizing systems activity between cells from the three mice lines, as follow: Ldlr^{Mut}Nnt^{Mut} > Nnt^{Mut} > Nnt^W. These findings demonstrate a gradient of oxidized

state when the cells have the Nnt mutation and both Nnt and Ldlr mutations. In order to check a possible participation of the enzyme NADPH oxidase (NOX), we used its inhibitor, the DPI (Figure 2B). DPI only had effect on the double mutant cells, decreasing DHE fluorescence by 25% ($P < 0.05$). The lack of effect of DPI in wild-type and Nnt single mutant cells suggest that NOX is not active in these cells, while cells obtained from double mutant mice have already a certain level of NOX activation.

Due to the high abundance of glutathione and its reactive oxygen scavenger ability, the ratio between reduced and oxidized glutathione (GSH/GSSG) is used as a marker of cell oxidative stress. Indeed, in Figure 2C we show a decrease in GSH/GSSG ratios in macrophage of both Nnt^{Mut} (single mutant) and Ldlr^{Mut}Nnt^{Mut} (double mutant) compared with Nnt^W (control) cells, in agreement with the observed increase in H₂O₂ (Figure 2A) and superoxide production rates (Figure 2B) in these cells.

To determine specific mitochondria redox state, macrophages were labeled with the MitoSOX red, a mitochondrial targeted DHE probe, followed by Mitotracker green, a green-fluorescent dye which localizes to mitochondria [38], and DAPI (nuclei dye). Images were captured by confocal microscopy. As shown in Figure 3, both mutant mice peritoneal macrophages present marked increased signal of both probes, MitoSOX and Mitotracker, suggesting a more oxidized state of mitochondria but also an increased number of mitochondria in these cells. Indeed, we observed significant increases in co-localized labeled areas in the macrophages from the mutant cells, as follow: Ldlr^{Mut}Nnt^{Mut} > Nnt^{Mut} > Nnt^W (control). To clarify whether mitochondria oxidants production or only mitochondria number were increased in the double and single Nnt mutant cells, we studied oxidants production in isolated mitochondria obtained from liver and heart of the three groups of mice (Figures 4 and 5). As expected, we confirmed that both mitochondria from Nnt and Nnt + Ldlr mutant mice have no capacity to sustain endogenous NADPH in the reduced state, unless isocitrate is provided to re-reduce NADP⁺ through isocitrate dehydrogenase (Supplementary Figure S1). Liver mitochondria from Nnt mutant and Nnt + Ldlr double mutant produced more H₂O₂ (Amplex red, Figure 4A,B) and global unspecific oxidants (DCF, Figure 4C,D) than the control mitochondria, in a graded manner, exactly as observed in macrophages: Ldlr^{Mut}Nnt^{Mut} > Nnt^{Mut} > Nnt^W. These results confirm higher oxidants production per mitochondria unit in both mutant mice. An indicator of protein oxidative damage (nitrotyrosine levels) is observed in the double mutant mitochondria compared with the single mutant and wild-type mitochondria (Supplementary Figure S2). Since both mutant mitochondria present higher oxidants production, it is expected that these organelles are more susceptible to mitochondria membrane permeability transition (MPT). Indeed, as shown in Figure 5, both mutant mitochondria are more susceptible to MPT, as measured by cyclosporine A (CsA) sensitive swelling (Figure 5A) and membrane potential dissipation after calcium challenge (Figure 5B,C). Again, in parallel with oxidants production, the same graded response is observed for MPT: Ldlr^{Mut}Nnt^{Mut} > Nnt^{Mut} > Nnt^W.

Experiments with Mitosox and Mitotracker (Figure 3) suggested an increased number of mitochondria in both mutant macrophages. Considering the higher rates of oxidants production and depleted GSH and NADPH levels in mutant cells, it is feasible to postulate that this oxidative condition could stimulate mitochondria biogenesis as a redox mechanism of mitochondrial self-protection [39]. We therefore focused on two proteins directly related to the mitochondrial biogenesis, the co-transcriptional factor PGC-1 α and the mitochondrial transcription factor A (TFAM). The latter drives transcription and replication of mitochondrial DNA. Figure 6A,B show Western blots of PGC-1 α and TFAM. Although results showed great variability among different samples ($n = 4$ /group), particularly regarding PGC-1 α , we could still detect statistical significant differences between mutants and wild-type cells. We found an increase in these protein expressions reproducing the same gradient observed for mitochondrial superoxide (MitoSox) and Mitotracker labels, as follow: Ldlr^{Mut}Nnt^{Mut} > Nnt^{Mut} > Nnt^W (Figure 6A,B). In the case of higher number of mitochondria in mutant macrophages, we should be able to detect higher expression levels of the oxidative phosphorylation (OXPHOS) protein complexes. In fact, we found that complex I, II and III are significantly increased in both mutant macrophages, Ldlr^{Mut}Nnt^{Mut} and Nnt^{Mut}, compared with control Nnt^W (Figure 6C,D). Together, whole cells and isolated mitochondria data indicate that both increased mitochondrial oxidants and increased mitochondria number are present in double and single Nnt mutant macrophages compared with controls.

The oxidative stress observed in both Nnt mutant macrophages is a feature of activated and pro-inflammatory type of macrophages found in early atherosclerosis lesions. Thus, we investigated the expression levels of inflammatory markers in these cells (Figure 7). Indeed, single and double mutant macrophages showed marked increases in the mRNA expression of inducible nitric oxide synthase (iNOS), interleukin-1 and 6, while no significant differences were observed in TNF α among the cells (Figure 7A). Confirming these results, the concentrations of interleukin-1 and 6 were also increased in the media of Nnt mutant macrophages (Figure 7B).

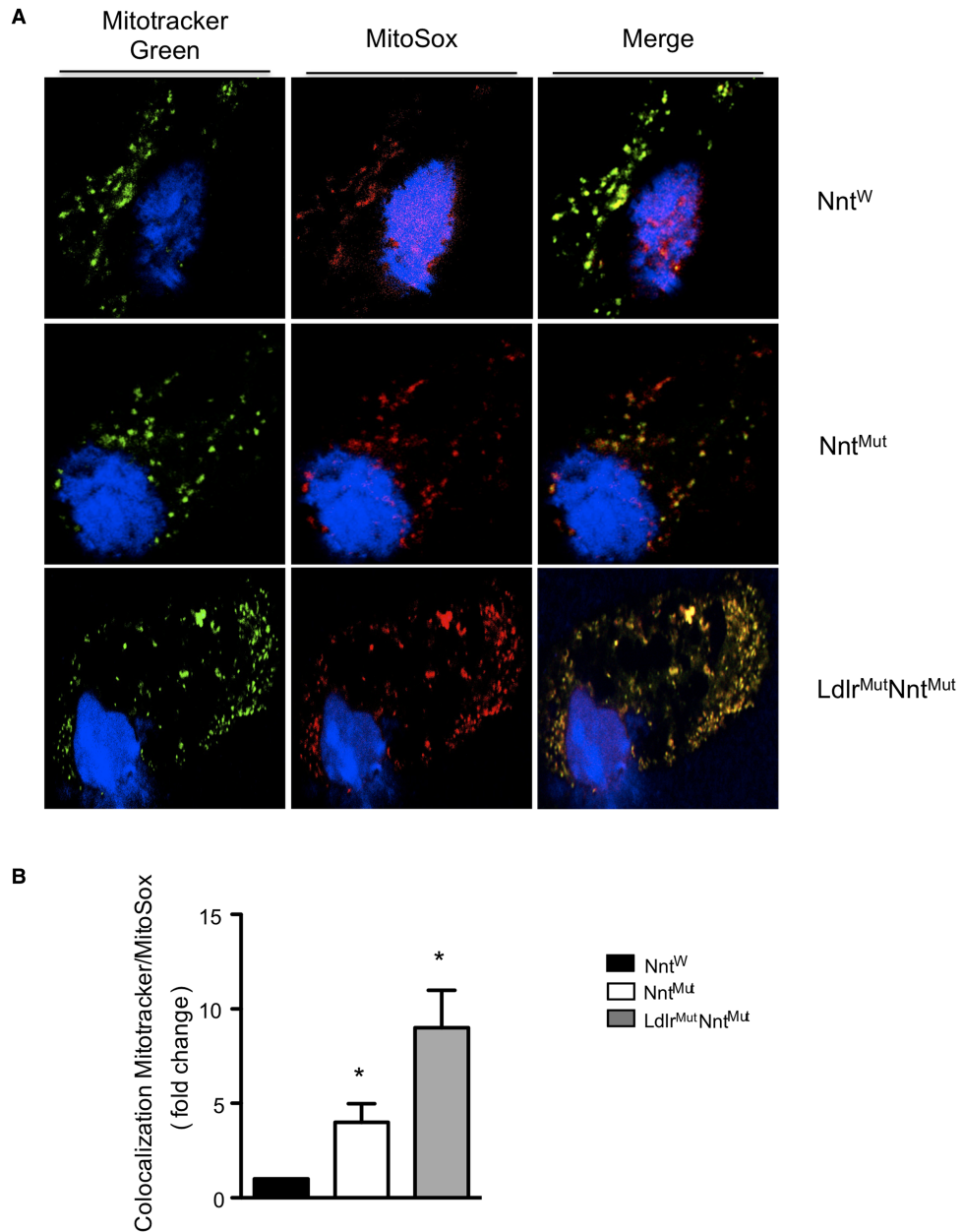


Figure 3. Nnt and Ldlr mutant macrophages present increased mitochondria number and redox imbalance.

(A) Representative images and (B) quantitation of mitochondria redox state (MitoSox red) and number (Mitotracker green). Nuclei were stained with DAPI. Images captured by fluorescence microscopy. Mean \pm SE ($n = 3$) * $P < 0.05$ vs Nnt^W (control), one-way ANOVA with Tukey's posttest.

We next studied the very early event that leads these cells to become foam cells. We measured acetylated-LDL (acLDL) and oxidized-LDL (oxLDL) derived intracellular lipid accumulation. After culturing mouse peritoneal macrophages with DiI-acLDL, a significant increase in fluorescent neutral lipids accumulation in both mutant macrophages were observed, 50% increase in Nnt^{Mut} and 2.3-fold increase in Ldlr^{Mut}Nnt^{Mut} compared with controls (Figure 8A,B). In addition, we measured directly the cholesterol mass taken up by the macrophages after incubation with oxLDL. We observed a 1.7- to 2-fold increase in the cholesterol uptake by both Nnt mutant cells (Figure 8C). We then determine the protein expression of membrane transporters involved in the uptake of modified lipoprotein (the scavenger receptors CD36, SRA, SRB-1) and in the cell

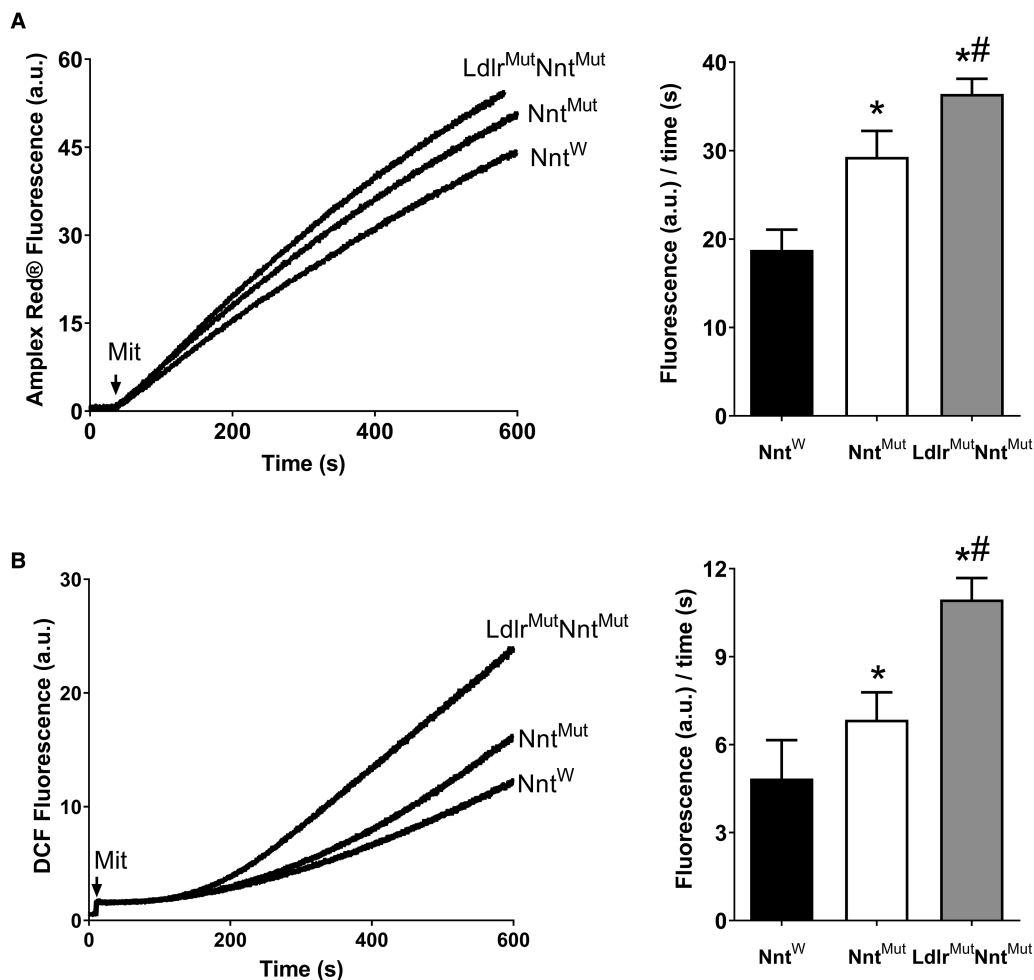


Figure 4. Generation of reactive oxygen species is increased in liver mitochondria from Nnt and Ldlr + Nnt mutant mice. Liver mitochondria were added to standard reaction medium containing Amplex red (A) or H₂-DCFDA (B) in the presence of 200 μ M EGTA. Quantitation was measured as maximum rates (slopes) of H₂O₂ (A) and global oxidants (B) production. Mean \pm SD ($n = 5$) * $P < 0.05$ vs Nnt^W, # $P < 0.05$ vs Nnt^{Mut}, one-way ANOVA with Tukey's posttest.

cholesterol efflux (the ABCA1 and G1 transporters) (Figure 9). Western blot analyses demonstrated that both Nnt mutant macrophages presented reduced levels of ABCA1, 33% in single mutant Nnt^{Mut} and 15% in double mutant Ldlr^{Mut}Nnt^{Mut} macrophage, but similar levels of ABCG1 and SRB-1, compared with the control Nnt^W cells (Figure 9A,B). The immunoblots for other macrophage scavenger receptors (CD36 and SRA) showed that both Nnt mutant cells present increased CD36 content (Figure 9C,D). Single Nnt^{Mut} cells had 50% increase in CD36 content, although statistical significance was not reached. Double mutant Ldlr^{Mut}Nnt^{Mut} macrophage exhibited a 3-fold increase in CD36 content. These findings can explain increased uptake and reduced efflux rates of modified LDL-cholesterol during foam cell formation in both Nnt mutant macrophages. We also determined the mRNA expression levels of CD36 and ABCA1 in the absence and presence of the antioxidant Tempo, a stable cell-permeable nitroxide that acts as a free radical scavenger (Figure 9E). It is observed that ABCA1, but not CD36, mRNA is down-regulated in double mutant cells and that this down-regulation is abolished by the antioxidant treatment.

To check whether these differential redox, inflammatory and cholesterol accumulation in Nnt mutant macrophages would be relevant for atherosclerosis, we performed transplantation of Ldlr^{-/-} recipient mice with bone marrow from Nnt^{Mut} and Nnt^W donor mice and measured diet-induced atherosclerosis in their aorta root (Figure 10). We observed that the group transplanted with wild-type Nnt bone marrow presents significantly smaller lipid stained lesions (26%) than the group that received the mutant Nnt bone marrow. Additional aorta

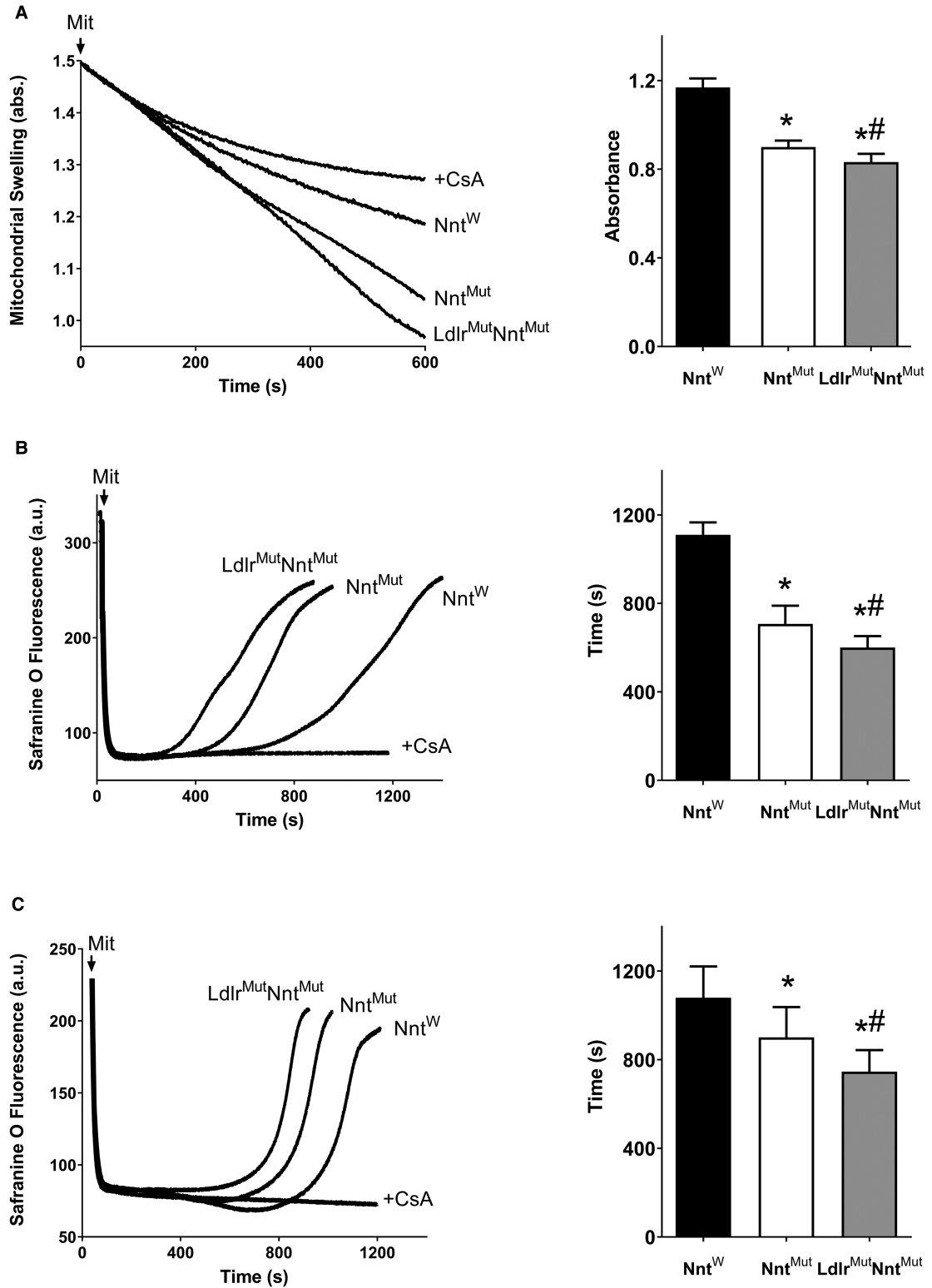


Figure 5. Susceptibility to mitochondrial permeability transition (MPT) is increased in mitochondria from Nnt and Ldlr + Nnt mutant mice.

Part 1 of 2

MPT was measured as cyclosporine A (CsA, 1 μ M) sensitive swelling (A) and membrane potential dissipation (B and C) induced by calcium. Liver (A and B) or heart (C) mitochondria (Mit., 0.5 mg/ml) were added to standard reaction medium, containing calcium (35 μ M). Swelling was followed by changes in mitochondrial solution turbidity at 520 nm. Quantitation

Figure 5. Susceptibility to mitochondrial permeability transition (MPT) is increased in mitochondria from Nnt and Ldlr + Nnt mutant mice.

Part 2 of 2

determined as the absorbance at 500 s after mitochondria addition, $n = 6$ (A). Changes in membrane electrical potential in mice liver, $n = 10$ (B) or heart, $n = 12$ (C) mitochondria were followed monitoring safranin O ($5 \mu\text{M}$) fluorescence. Quantitation was determined as the lag time to start dissipation of membrane electrical potential. Mean \pm SD, * $P < 0.05$ vs Nnt^{W} , # $P < 0.05$ vs Nnt^{Mut} , one-way ANOVA with Tukey's posttest.

root sections were immune-staining for CD68 (macrophages) and nitrotyrosine (3-NT), an indicator of cell oxidative damage and inflammation mediated by reactive nitrogen species such as peroxynitrite anion (Figure 10B,C). We observed a 50% reduction in 3-NT content and 36% reduction in macrophage content in lesions of mice that received the wild-type Nnt bone marrow. Therefore, the severity of atherosclerosis matches with oxidants

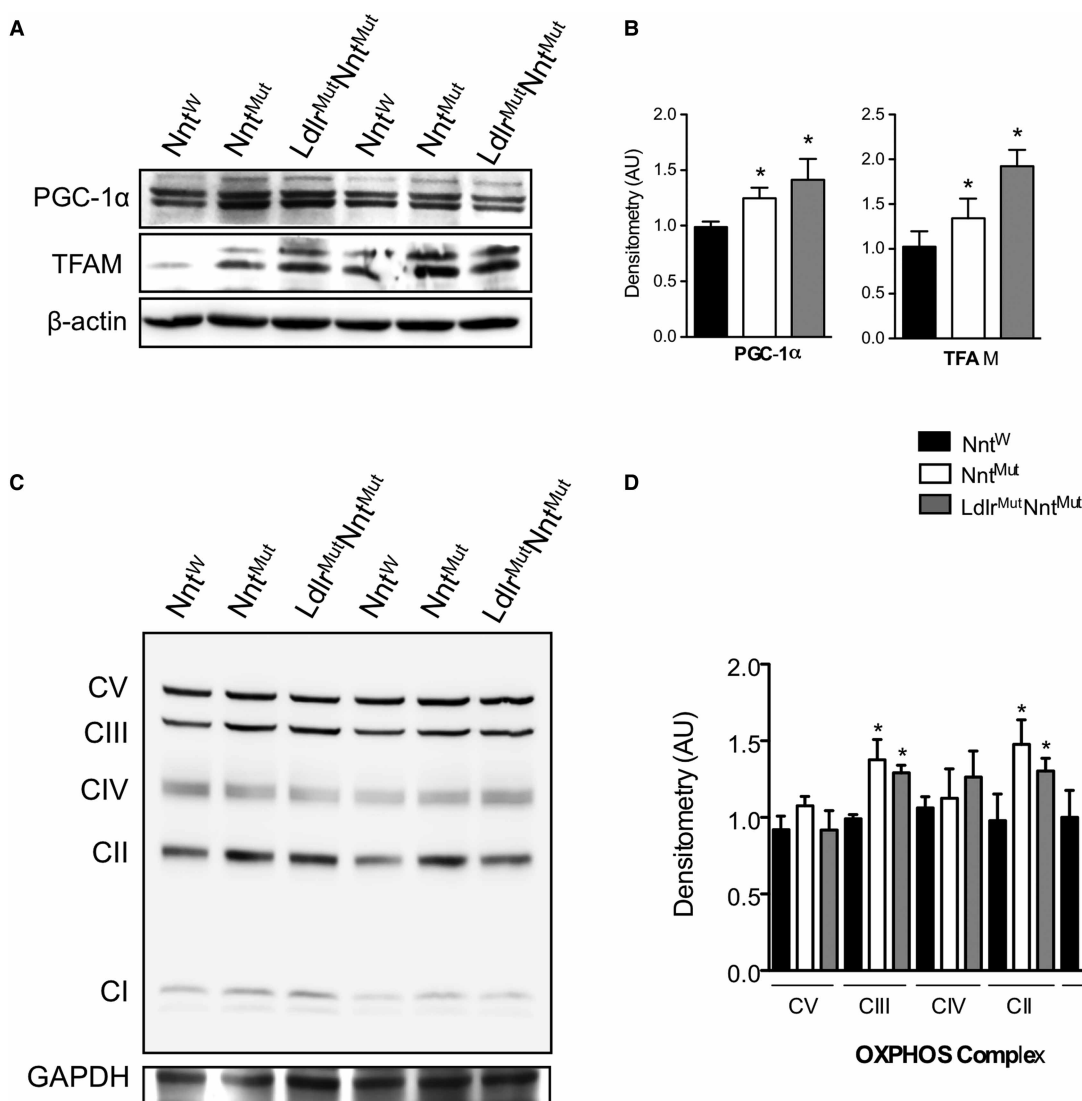


Figure 6. Nnt and Ldlr mutant macrophages present increased levels of mitochondria biogenesis markers.

Expression levels of PGC-1 α and TFAM (A and B) and mitochondrial oxidative phosphorylation complexes (C and D). Mean \pm SE ($n = 4-5$). * $P < 0.05$ vs Nnt^{W} (control), one-way ANOVA with Tukey's posttest.

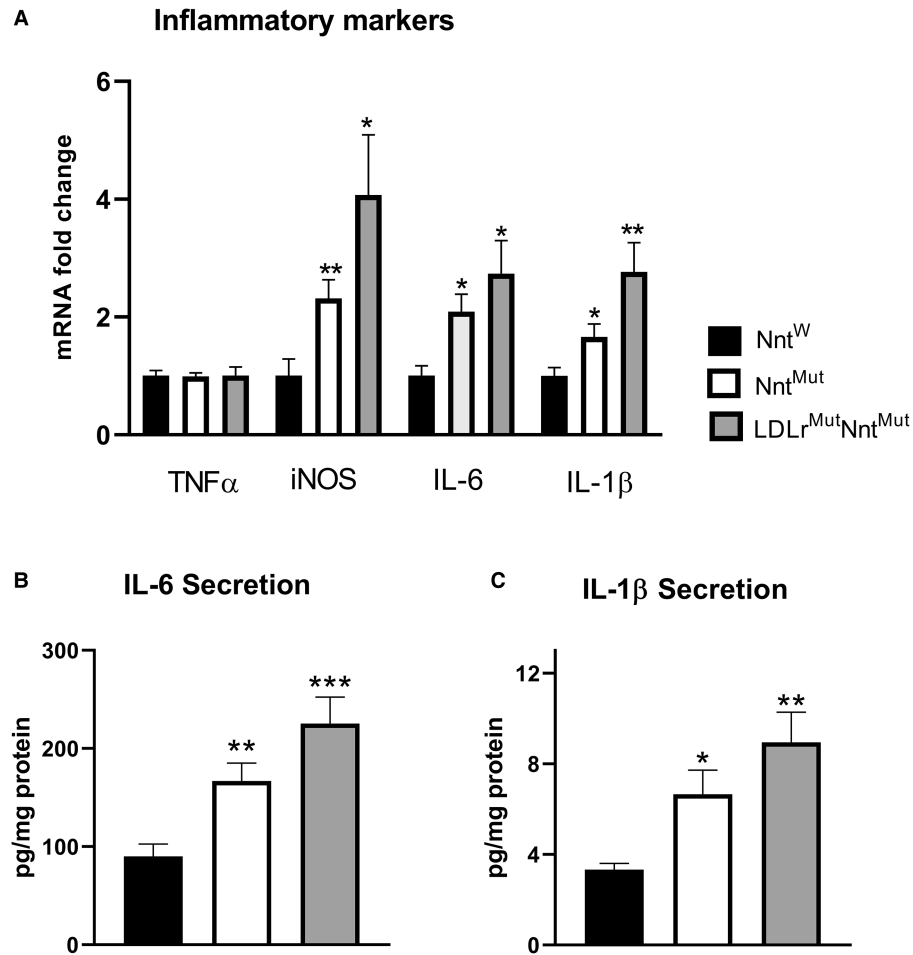


Figure 7. Nnt and Ldlr mutant macrophages present increased levels of inflammatory markers.

mRNA expression (normalized by 36B4) of tumor necrosis factor alpha (TNF α), inducible nitric oxide synthase (iNOS) and interleukin 6 and 1 beta (IL-6 and IL-1 β) were determined by RT-PCR (A). IL-6 and IL-1 β secretion into the media were determined by ELISA (R&D Systems and Invitrogen, respectively) (B and C). Mean \pm SE ($n = 5-10$). * $P < 0.05$, ** $P < 0.01$, *** $P < 0.001$ vs Nnt^W, one-way ANOVA with Tukey's posttest.

production, inflammatory markers expression and secretion and foam cell formation observed in isolated macrophages.

Plasma cholesterol and triglycerides (TG) levels could play a determinant role in disease severity of transplanted mice. Thus, we measured plasma lipids at the end of the transplantation experiments (Supplementary Table S2). Plasma cholesterol and TG levels were similar in mutant and wild-type Nnt bone marrow transplanted mice, thus ruling out a cholesterol effect on their lesion size. In addition, plasma lipoprotein profiles of Nnt mutant and wild-type donor mice were evaluated (Supplementary Figure S3). The data show no significant differences between the lipoprotein profile of the Nnt^{Mut} and Nnt^W mice, as expected.

Discussion

Although the Nnt spontaneous mutation in the C57BL/6J mice occurred ~ 30 years ago [40], its discovery was only reported in 2005 [19]. Compared with Nnt wild-type independent or closely related strains, C57BL/6J mice present quite distinct metabolic phenotypes, including impaired glucose tolerance and reduced glucose-stimulated insulin secretion [19,21–23,41,42]. In addition, these Nnt deficient mice are more susceptible to obesity, heart failure and hypertension [25,29,43]. Considering that atherogenesis is triggered by a local oxidative stress, that mitochondria are major sources of reactive oxygen in eukaryotic cells, and that Nnt provides reducing power (NADPH) for detoxifying mitochondria H₂O₂, we hypothesized that Nnt deficiency

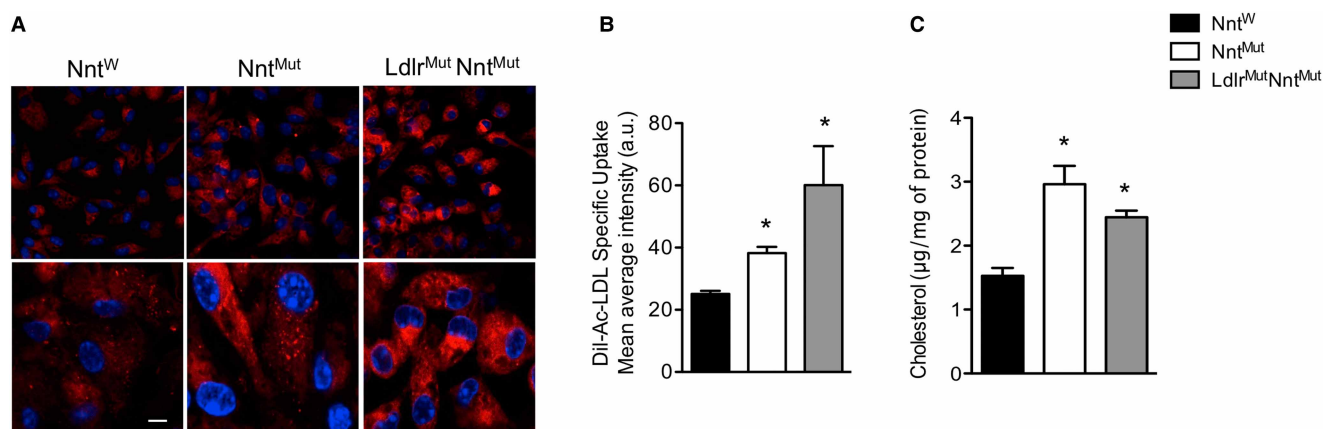


Figure 8. Increased foam cell formation in Nnt and Ldlr mutant macrophages.

Acetylated-LDL induced lipid accumulation (A and B) and oxidized LDL induced cholesterol uptake (C). (A) Representative micrographs from peritoneal macrophages incubated with DiI-Ac-LDL (30 µg/ml) for 2 h at 37°C; nuclei were counterstained with DAPI. Scale bar: 10 µm. Magnification 20× and 63×. (B) Lipid accumulation measured as median intensity fluorescence (M.I.F.) of DiI; (C) cholesterol uptake after incubation of peritoneal macrophages with oxLDL (60 µg/ml) for 6 h at 37°C. Cell cholesterol content was measured using the enzymatic-fluorimetric Amplex red kit. Mean ± SE ($n = 4-5$). * $P < 0.05$ vs Nnt^W (control), one-way ANOVA with Tukey's posttest.

would impact on the initiation and progression of atherosclerosis. To test this hypothesis we focus our study on macrophages from single Nnt and double Nnt + Ldlr mutant mice. As expected, we found additive redox imbalance effects in single Nnt mutant cells (lower NADPH production) and double Nnt + Ldlr mutant cells (lower production + higher consumption of NADPH for steroidogenesis), as well as a stimulating effect of Nnt deficiency on inflammation and foam cell formation (*in vitro*) and atherosclerosis development (*in vivo*).

We reported previously in isolated liver mitochondria that the specific activity of Nnt was nearly absent from Nnt^{Mut} mitochondria compared with control (Nnt^W), with several consequences for mitochondrial redox homeostasis, including a decrease in GSH levels and higher rates of H₂O₂ release [35]. In the present study, we confirmed that these redox alterations induced by the Nnt mutation also occur in whole cells and further expanded the findings showing the impact of Nnt and Ldlr mutations on the macrophage mitochondria biogenesis, inflammation and cholesterol homeostasis. Nnt and Ldlr mutations caused an imbalance in the cell redox state, increased mitochondrial biogenesis (PGC1α and TFAM expression), inflammation (iNOS, IL-1 and IL-6) and lipid accumulation (foam cell formation). Besides, Nnt mutation decreased cell GSH/GSSG ratio (reducing power) and ABCA1 expression (cholesterol efflux), while Ldlr + Nnt mutations caused up-regulation of SOD2 and CD36 (cholesterol uptake). Thus, confirming our hypothesis, Nnt and Ldlr mutations led to a graded exacerbation of the process of foam cell formation induced by chemically modified LDL.

Mitochondrial biogenesis is stimulated by environmental conditions of high energy demand and in disease threatening conditions, such as during inflammatory and degenerative processes, as a homeostatic mechanism [44,45]. An intracellular increase in oxidants production may cause simultaneous induction of mitochondrial biogenesis and antioxidant gene expression [39,45], such as those observed in Nnt and Ldlr + Nnt mutant macrophages. However, mitochondria biogenesis in these mutant macrophages were not able to compensate for the pro-oxidant status since they have a genetic defective NADPH production to detoxify H₂O₂, rendering them more susceptible to redox imbalance and lipid accumulation.

Oxidative stress conditions, including mitochondrial redox dysfunction, can provoke and potentiate inflammatory response, a key event in atherosclerosis. Previous studies indicate that increased oxidants production can induce the assembly of inflammasomes, which triggers the caspase-1-mediated maturation of the precursors of IL-1β [46]. Interleukin-6 (IL-6) is an upstream inflammatory cytokine that plays a central role in propagating the downstream inflammatory response in atherosclerosis [47] and a large body of evidence suggests that IL-1 signaling is proatherogenic [48]. Induction of iNOS usually occurs in an oxidative and/or inflammatory environment [49,50], and thus high levels of NO react with nearby superoxide leading to the formation of the potent oxidant peroxynitrite and consequent protein nitration and cell toxicity. In fact, we found elevated levels of nitrotyrosine in proteins of isolated Nnt mutant mitochondria and in the aorta lesions of mice transplanted

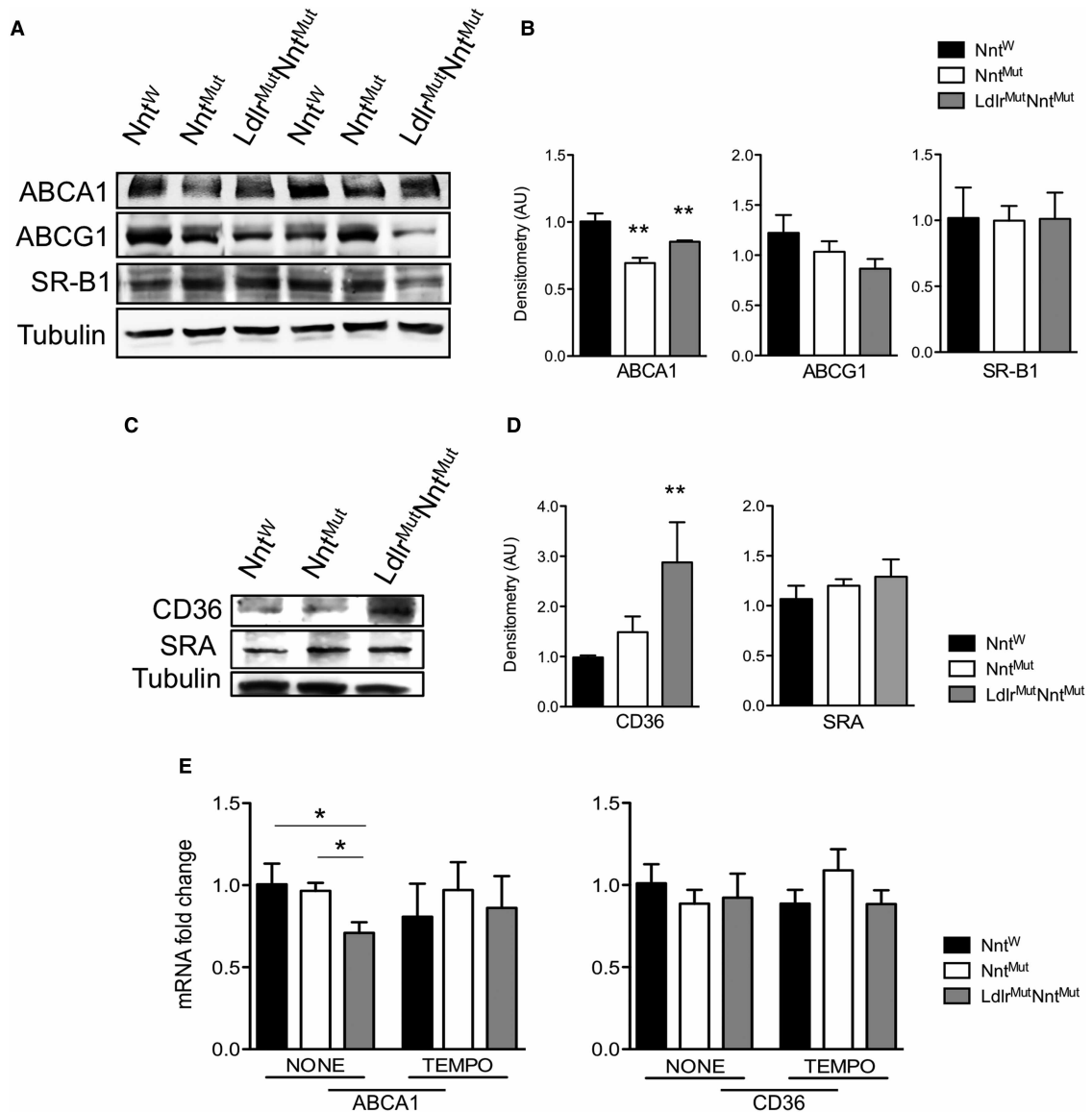


Figure 9. Expression of cholesterol membrane efflux mediators (ABCA1 and G1) and scavenger receptors (SRB-1, CD36, SRA) in Nnt and Ldlr mutant macrophages.

Immunoblots of ABCA1, ABCG1, and SR-B1 transporters (**A** and **B**); Immunoblots of CD36 and SRA scavenger receptors (**C** and **D**); mRNA expression of CD36 and ABCA1 (normalized by 36B4) before and after incubation (24 h) with the antioxidant Tempo (50 μ M) (**E**). Mean \pm SE ($n = 3-5$ for blots and $n = 5-8$ for RT-PCR), * $P < 0.05$ vs Nnt^W (control), one-way ANOVA with Fisher LSD test; ** $P < 0.05$ vs Nnt^W (control), Student's *t*-test.

with Nnt mutant macrophages. It is possible that in the Nnt mutant cells, iNOS itself also catalyzes the superoxide production at the expense of NADPH, thus boosting peroxynitrite generation [51].

The disruption of macrophage cholesterol homeostasis induced by Nnt deficiency relies on, at least in part, the down-regulation of the ATP-binding cassette (ABC) transporters-A1 (ABCA1) expression, an unsuspected novel finding. ABCA1 transporters mediate cell cholesterol efflux, a process relevant for preventing initiation and accelerating regression of atherosclerosis. ABCA1 expression is positively regulated by liver X receptor (LXR) transcription factor activity [52]. It is possible that Nnt mutation dependent oxidants production led to down-regulation of LXR and consequently of the ABCA1 expression, such as previously described for human neutrophils and macrophages treated with an inflammatory mediator, deoxy-prostaglandin J2 (dPGJ2) [53].

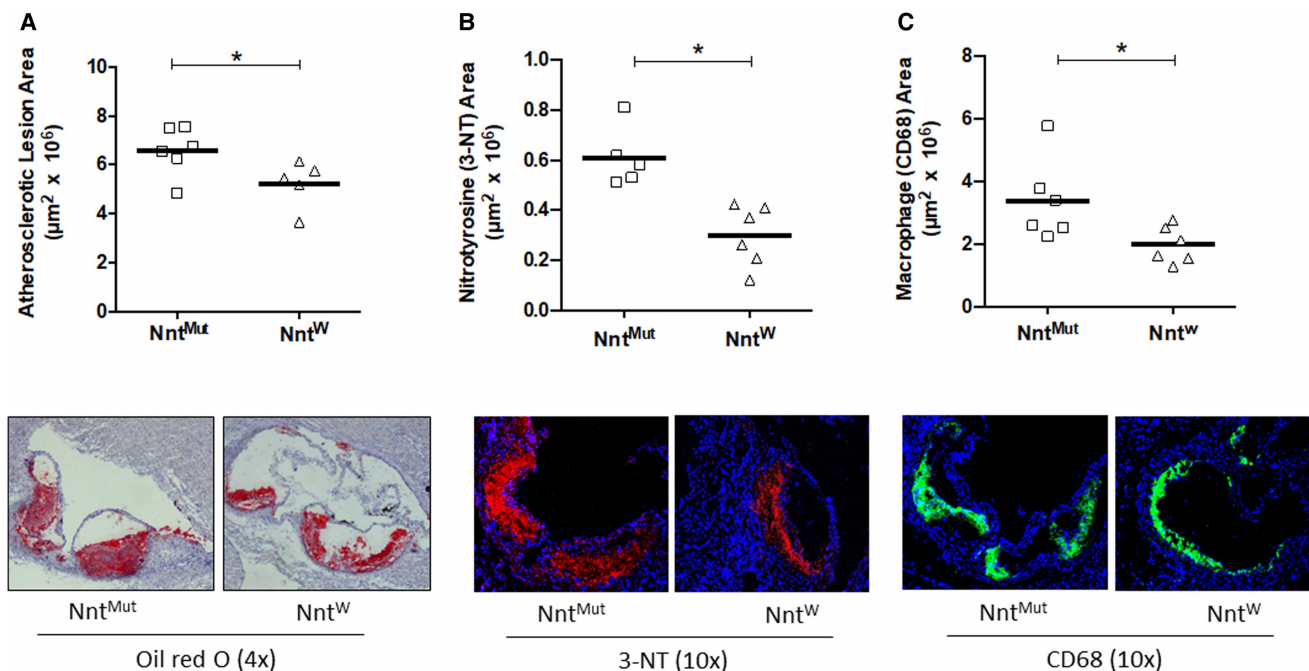


Figure 10. Aorta atherosclerotic lesions are decreased in *Ldlr*^{-/-} mice transplanted with wild-type macrophages (*Nnt*^W).

Ldlr^{-/-} mice were transplanted with bone marrow from the two donor mice line: *Nnt*^{Mut} and *Nnt*^W. Transplantation occurred 1 day after irradiation and, one week after recovery, transplanted mice were placed on a western type diet for 8 weeks. Atherosclerosis was measured as Oil red O lipid stained (A), nitrotyrosine (B) and macrophages (CD68) (C) immuno-stained sections of aorta root of *Ldlr*^{-/-} recipient mice. Representative images of the stained lesions are shown in the bottom panels. *N* = 5–6 and * *P* < 0.05 by Student's *t*-test.

This down-regulatory effect was dependent on the release of reactive oxygen species elicited by dPGJ2, since it was reversed by antioxidants [53]. Here, we showed that a genetic deficiency of the *Nnt*, without any other exogenous pro-oxidant, elicits mitochondrial redox imbalance in macrophages and hinder ABCA1 mediated cholesterol efflux, favoring cell lipid accumulation. Confirming redox regulation of ABCA1 gene, the down-regulation of its mRNA observed in the *Nnt* + *Ldlr* mutant macrophages was abolished by an antioxidant treatment. In addition to redox regulation, inflammation itself may inhibit ABCA1 expression [54,55].

Cell surface CD36 protein is a member of the scavenger receptor family that binds to and internalize modified LDL particles, thereby facilitating macrophage cholesterol influx capacity and foam cell formation. We showed in this study that *Nnt* and *Ldlr* mutations have synergistic effects on increasing CD36 expression. In agreement with our data, it was previously described that pharmacological inhibition of GSH production, that lead to decreased GSH/GSSG and increased production of oxidants, was associated with up-regulation of macrophage CD36 expression (at the translational level) and enhanced cellular oxidized LDL uptake [56]. Therefore, it seems that CD36 protein is regulated by the macrophage antioxidant capacity, which in the *Nnt* and *Ldlr* mutant macrophages is affected by the low GSH and NADPH content. It is likely that the additive effects of both mutations resulted in synergistic up-regulation of CD36 protein observed in *Nnt* + *Ldlr* double mutant macrophage. CD36 up-regulation together with ABCA1 down-regulation resulted in exacerbation of the process of foam cell formation.

Bone marrow transplantation of *Ldlr*^{-/-} mice experiments were designed to demonstrate that the impaired redox, inflammatory and cholesterol homeostasis in *Nnt* mutant macrophages would be relevant for atherosclerosis development. We demonstrated that aorta lesions in mice transplanted with *Nnt*^W macrophages was significantly diminished compared with those transplanted with *Nnt*^{Mut} macrophages, indicating that replenishing mice with macrophages with fully active *Nnt* attenuates atherosclerosis. A recent published paper [57] reported that the *Nnt* deficient C57BL/6J mice presented more diet-induced atherosclerosis than an independent *Nnt* expressing C57BL/6N mice line. Both groups were made hypercholesterolemic by an adenovirus mediated overexpression of the PCSK9 (proprotein convertase subtilisin/kexin type 9). Although this report is

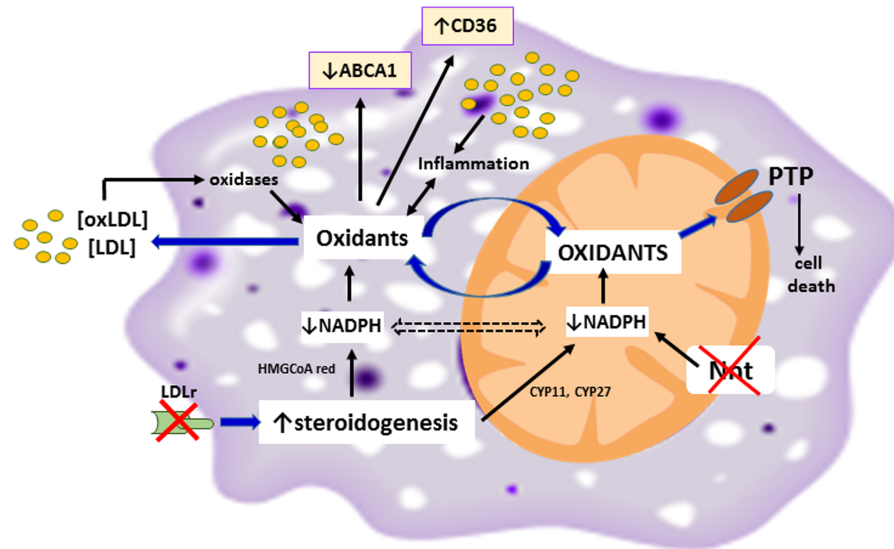


Figure 11. Proposed model to explain how LDLr and Nnt deficiencies in macrophages predispose to atherogenesis.

LDLr deficiency induces compensatory increase in cholesterol synthesis and metabolism. Thus, several pathways that consume reducing power (NADPH) are up-regulated such as mevalonate (HMGCoA reductase) and cholesterol oxidation (CYP11/27). Decreased mitochondria NADPH due to Nnt deficiency impairs mitochondrial antioxidant enzymatic system and favors oxidant accumulation and permeability transition pore (PTP) formation. Permeable mitochondrial and cell oxidants may directly attack LDL, generating oxLDL, which in turn are taken up by cells and activate extra mitochondrial oxygenases favoring oxidant production. Oxidative stress induces inflammation. High levels of oxidants regulate membrane cholesterol transporters such as CD36 (translation) and ABCA1 (transcription).

in line with our results, it is blurred by an experimental design flaw. These two independent mice lines constitute fully distinct metabolic settings that *per se* are known to influence atherosclerosis. Compared with BL/6N mice, the Nnt deficient BL/6J mice are glucose intolerant, insulin resistant, and more susceptible to obesity, inflammation and hypertension [25,26,29,42]. Endothelial dysfunction, that imposes a major impact on atherosclerosis development, is likely present in the BL/6J (Nnt deficient) mice but not in the BL/6N (intact Nnt) mice. Thus, many atherosclerosis predisposing conditions were differentially present in these two experimental groups. In the present study, we evaluate atherosclerosis development in a entirely homogeneous genetic and metabolic background (BL/6J), Nnt deficient in the whole body, including the endothelium; groups differed exclusively by the replenishment of macrophages expressing Nnt or not.

In summary, these data provide evidence that the lack of Nnt in macrophages increases foam cell formation *in vitro* and atherosclerosis severity *in vivo*, and conversely, replenishing deficient mice with Nnt expressing macrophages decreases atherosclerosis. In addition, we showed that the lack of Nnt is involved not only in mitochondrial redox imbalance but also in the up-regulation of inflammatory effectors and alterations of proteins responsible for cell cholesterol accumulation (decreased ABCA1 and increased CD36). Our proposed model to put these data together is shown in Figure 11. Putting these findings into perspective, the functionality of Nnt (perhaps verified by Nnt gene polymorphisms) or the availability of reducing power (NADPH and GSH) in mononuclear cells are relevant factors for atherosclerosis risk. These data support therapeutic strategies such as inhibition of steroidogenesis (statins) that would spare reducing power and/or treatment with safe antioxidants to compensate for low reducing power conditions. Nonetheless, these findings have yet to be translated to human disease.

Abbreviations

ABCA1, ATP binding cassette A1 transporter; ABCG1, ATP binding cassette G1 transporter; CD36, scavenger receptor class B member 3; DCF, dichlorofluorescein; DHE, dihydroethidium; GSH, reduced glutathione; GSSG, oxidized glutathione; H₂-DCFDA, 2',7'-dichlorodihydrofluorescein diacetate; HMG-CoA reductase, 3-hydroxi-3-methyl-glutaril-CoA reductase; LDL, low-density lipoprotein; Ldlr^{-/-}, LDL receptor knockout mice;

Ldlr^{Mut}Nnt^{Mut}, double mutant, for LDLr and Nnt genes; LXR, liver X receptor; MPT, mitochondrial permeability transition; Nnt, nicotinamide nucleotide transhydrogenase or NAD(P)H transhydrogenase; Nnt^{Mut}, mutant for the Nnt gene; Nnt^W, wild type for the Nnt gene; OXPHOS, oxidative phosphorylation; PCSK9, proprotein convertase subtilisin/kexin type 9; PGC-1 α , PPAR gamma co-transcriptional activator 1 α ; SOD2, mitochondrial manganese-dependent superoxide dismutase; SRA, scavenger receptor class A; SRB-1, scavenger receptor class B type 1; TFAM, mitochondrial transcription factor A; Trx, thioredoxin.

Author Contribution

A.G.S., T.R., G.G.D., E.L.G., A.C.B.A.W.: data collection, analysis and interpretation of all cell culture experiments; A.C.M., A.M.: data collection, analysis and interpretation of isolated mitochondria experiments; T.R. and G.G.D.: data collection, analysis and interpretation of bone marrow transplantation and diet induced atherosclerosis experiments; A.E.V.: designed and supervised mitochondria experiments, analyzed the data and provided intellectual contributions to the manuscript; A.G.S., H.C.F.O.: conceived the study, analyzed the data and wrote the manuscript; All authors contributed with and approved the final version of the manuscript.

Funding

This work was supported by grants from the Fundação de Amparo à Pesquisa do Estado de São Paulo to AEV and HCFO (FAPESP # 2011/50400-0, # 2013/07607-8 and # 2017/17728-8). AGS (#13/05497-0), ACM (#11/15103-4), ACBAW (#13/05497-0), AM (#11/15101-1) and GGD (#17/02903-9) were supported by FAPESP fellowships and T.R. and E.L.G. were supported by CAPES (Coordenação de Aperfeiçoamento de Pessoal de Nível Superior) fellowships.

Acknowledgements

We are grateful to Leonardo Moi de Carvalho for technical assistance.

Competing Interests

The authors declare that there are no competing interests associated with the manuscript.

References

- 1 Que, X., Hung, M.Y., Yeang, C., Gonen, A., Prohaska, T.A., Sun, X. et al. (2018) Oxidized phospholipids are proinflammatory and proatherogenic in hypercholesterolaemic mice. *Nature* **558**, 301–306 <https://doi.org/10.1038/s41586-018-0198-8>
- 2 Steinberg, D. (2009) The LDL modification hypothesis of atherogenesis: an update. *J. Lipid Res.* **50**, S376–S381 <https://doi.org/10.1194/jlr.R800087-JLR200>
- 3 Moore, K.J., Sheedy, F.J. and Fisher, E.A. (2013) Macrophages in atherosclerosis: a dynamic balance. *Nat. Rev. Immunol.* **13**, 709–721 <https://doi.org/10.1038/nri3520>
- 4 Yurdagül, Jr, A., Finney, A.C., Woolard, M.D. and Orr, A.W. (2016) The arterial microenvironment: the where and why of atherosclerosis. *Biochem. J.* **473**, 1281–1295 <https://doi.org/10.1042/BJ20150844>
- 5 Schieber, M. and Chandel, N.S. (2014) ROS function in redox signaling and oxidative stress. *Curr. Biol.* **24**, R453–R462 <https://doi.org/10.1016/j.cub.2014.03.034>
- 6 Dorighello, G.G., Paim, B.A., Kihl, S.F., Ferreira, M.S., Catharino, R.R., Vercesi, A.E. et al. (2016) Correlation between mitochondrial reactive oxygen and severity of atherosclerosis. *Oxid. Med. Cell. Long.* **2016**, 7843685 <https://doi.org/10.1155/2016/7843685>
- 7 Dorighello, G.G., Paim, B.A., Leite, A.C., Vercesi, A.E. and Oliveira, H.C. (2017) Spontaneous experimental atherosclerosis in hypercholesterolemic mice advances with ageing and correlates with mitochondrial reactive oxygen species. *Exp. Gerontol.* **109**, 47–50 <https://doi.org/10.1016/j.exger.2017.02.010>
- 8 Wang, Y., Wang, G.Z., Rabinovitch, P.S. and Tabas, I. (2014) Macrophage mitochondrial oxidative stress promotes atherosclerosis and nuclear factor- κ B-mediated inflammation in macrophages. *Circ. Res.* **114**, 421–433 <https://doi.org/10.1161/CIRCRESAHA.114.302153>
- 9 Zhang, H., Luo, Y., Zhang, W., He, Y., Dai, S., Zhang, R. et al. (2007) Endothelial-specific expression of mitochondrial thioredoxin improves endothelial cell function and reduces atherosclerotic lesions. *Am. J. Pathol.* **170**, 1108–1120 <https://doi.org/10.2353/ajpath.2007.060960>
- 10 Madamanchi, N.R. and Runge, M.S. (2007) Mitochondrial dysfunction in atherosclerosis. *Circ. Res.* **100**, 460–473 <https://doi.org/10.1161/01.RES.0000258450.44413.96>
- 11 Yu, E.P. and Bennett, M.R. (2014) Mitochondrial DNA damage and atherosclerosis. *Trends Endocrinol. Metab.* **25**, 481–487 <https://doi.org/10.1016/j.tem.2014.06.008>
- 12 Harrison, C.M., Pompilius, M., Pinkerton, K.E. and Ballinger, S.W. (2011) Mitochondrial oxidative stress significantly influences atherogenic risk and cytokine-induced oxidant production. *Environ. Health Persp.* **119**, 676–681 <https://doi.org/10.1289/ehp.1002857>
- 13 Hunter, D.R., Haworth, R.A. and Southard, J.H. (1976) Relationship between configuration, function, and permeability in calcium-treated mitochondria. *J. Biol. Chem.* **251**, 5069–5077 PMID:134035
- 14 Figueira, T.R., Barros, M.H., Camargo, A.A., Castilho, R.F., Ferreira, J.C.B., Kowaltowski, A.J. et al. (2013) Mitochondria as a source of reactive oxygen and nitrogen species: from molecular mechanisms to human health. *Antioxid. Redox Signal.* **18**, 2029–2074 <https://doi.org/10.1089/ars.2012.4729>
- 15 Hoek, J.B. and Rysdrom, J. (1988) Physiological roles of nicotinamide nucleotide transhydrogenase. *Biochem. J.* **254**, 1–10 <https://doi.org/10.1042/bj2540001>

- 16 Pedersen, A., Karlsson, G.B. and Rydstrom, J. (2008) Proton-translocating transhydrogenase: an update of unsolved and controversial issues. *J. Bioenerg. Biomembr.* **40**, 463–473 <https://doi.org/10.1007/s10863-008-9170-x>
- 17 Arkblad, E.L., Tuck, S., Pestov, N.B., Dmitriev, R.I., Kostina, M.B., Stenvall, J. et al. (2005) A *Caenorhabditis elegans* mutant lacking functional nicotinamide nucleotide transhydrogenase displays increased sensitivity to oxidative stress. *Free Radic. Biol. Med.* **38**, 1518–1525 <https://doi.org/10.1016/j.freeradbiomed.2005.02.012>
- 18 Sheeran, F.L., Rydstrom, J., Shakhparonov, M.I., Pestov, N.B. and Pepe, S. (2010) Diminished NADPH transhydrogenase activity and mitochondrial redox regulation in human failing myocardium. *Biochim. Biophys. Acta* **1797**, 1138–1148 <https://doi.org/10.1016/j.bbabi.2010.04.002>
- 19 Toye, A.A., Lippiat, J.D., Proks, P., Shimomura, K., Bentley, L., Huggill, A. et al. (2005) A genetic and physiological study of impaired glucose homeostasis control in C57BL/6J mice. *Diabetologia* **48**, 675–686 <https://doi.org/10.1007/s00125-005-1680-z>
- 20 Huang, T.T., Naeemuddin, M., Elchuri, S., Yamaguchi, M., Kozy, H.M., Carlson, E.J. et al. (2006) Genetic modifiers of the phenotype of mice deficient in mitochondrial superoxide dismutase. *Hum. Mol. Genet.* **15**, 1187–1194 <https://doi.org/10.1093/hmg/ddl034>
- 21 Freeman, H.C., Huggill, A., Dear, N.T., Ashcroft, F.M. and Cox, R.D. (2006) Deletion of nicotinamide nucleotide transhydrogenase: a new quantitative trait locus accounting for glucose intolerance in C57BL/6J mice. *Diabetes* **55**, 2153–2156 <https://doi.org/10.2337/db06-0358>
- 22 Santos, L.R.B., Muller, C., de Souza, A.H., Takahashi, H.K., Spegel, P., Sweet, I.R. et al. (2017) NNT reverse mode of operation mediates glucose control of mitochondrial NADPH and glutathione redox state in mouse pancreatic beta-cells. *Mol. Metab.* **6**, 535–547 <https://doi.org/10.1016/j.molmet.2017.04.004>
- 23 Shimomura, K., Galvanovskis, J., Goldsworthy, M., Huggill, A., Kaizak, S., Lee, A. et al. (2009) Insulin secretion from beta-cells is affected by deletion of nicotinamide nucleotide transhydrogenase. *Methods Enzymol.* **457**, 451–481 [https://doi.org/10.1016/S0076-6879\(09\)05025-3](https://doi.org/10.1016/S0076-6879(09)05025-3)
- 24 Rydstrom, J. (2006) Mitochondrial transhydrogenase—a key enzyme in insulin secretion and, potentially, diabetes. *Trends Biochem. Sci.* **31**, 355–358 <https://doi.org/10.1016/j.tibs.2006.05.003>
- 25 Leskov, I., Neville, A., Shen, X.G., Pardue, S., Kevil, C.G., Granger, D.N. et al. (2017) Nicotinamide nucleotide transhydrogenase activity impacts mitochondrial redox balance and the development of hypertension in mice. *J. Am. Soc. Hypertension* **11**, 110–121 <https://doi.org/10.1016/j.jash.2016.12.002>
- 26 Ripoll, V.M., Meadows, N.A., Bangert, M., Lee, A.W., Kadioglu, A. and Cox, R.D. (2012) Nicotinamide nucleotide transhydrogenase (NNT) acts as a novel modulator of macrophage inflammatory responses. *FASEB J.* **26**, 3550–3562 <https://doi.org/10.1096/fj.11-199935>
- 27 Oliveira, H.C.F., Cosso, R.G., Alberici, L.C., Maciel, E.N., Salerno, A.G., Dorigheolo, G.G. et al. (2004) Oxidative stress in atherosclerosis-prone mouse is due to low antioxidant capacity of mitochondria. *FASEB J.* **18**, 278–280 <https://doi.org/10.1096/fj.04-2095fje>
- 28 Kogan, S.C., Doherty, M. and Gitschier, J. (1987) An improved method for prenatal diagnosis of genetic diseases by analysis of amplified DNA sequences. Application to hemophilia A. *N. Engl. J. Med.* **317**, 985–990 <https://doi.org/10.1056/NEJM198710153171603>
- 29 Nicholson, A., Reifsnnyder, P.C., Malcolm, R.D., Lucas, C.A., MacGregor, G.R., Zhang, W.D. et al. (2010) Diet-induced obesity in two C57BL/6 substrains with intact or mutant nicotinamide nucleotide transhydrogenase (Nnt) gene. *Obesity* **18**, 1902–1905 <https://doi.org/10.1038/oby.2009.477>
- 30 Ramkhalawon, B., Hennessy, E.J., Menager, M., Ray, T.D., Sheedy, F.J., Hutchison, S. et al. (2014) Netrin-1 promotes adipose tissue macrophage retention and insulin resistance in obesity. *Nat. Med.* **20**, 377–384 <https://doi.org/10.1038/nm.3467>
- 31 Hissin, P.J. and Hilf, R. (1976) A fluorometric method for determination of oxidized and reduced glutathione in tissues. *Anal. Biochem.* **74**, 214–226 [https://doi.org/10.1016/0003-2697\(76\)90326-2](https://doi.org/10.1016/0003-2697(76)90326-2)
- 32 Robinet, P., Wang, Z., Hazen, S.L. and Smith, J.D. (2010) A simple and sensitive enzymatic method for cholesterol quantification in macrophages and foam cells. *J. Lipid Res.* **51**, 3364–3369 <https://doi.org/10.1194/jlr.D007336>
- 33 Chu, E.M., Tai, D.C., Beer, J.L. and Hill, J.S. (2013) Macrophage heterogeneity and cholesterol homeostasis: classically-activated macrophages are associated with reduced cholesterol accumulation following treatment with oxidized LDL. *Biochim. Biophys. Acta* **1831**, 378–386 <https://doi.org/10.1016/j.bbailip.2012.10.009>
- 34 Kaplan, R.S. and Pedersen, P.L. (1983) Characterization of phosphate efflux pathways in rat-liver mitochondria. *Biochem. J.* **212**, 279–288 <https://doi.org/10.1042/Bj2120279>
- 35 Ronchi, J.A., Figueira, T.R., Ravagnani, F.G., Oliveira, H.C.F., Vercesi, A.E. and Castilho, R.F. (2013) A spontaneous mutation in the nicotinamide nucleotide transhydrogenase gene of C57BL/6J mice results in mitochondrial redox abnormalities. *Free Radic. Biol. Med.* **63**, 446–456 <https://doi.org/10.1016/j.freeradbiomed.2013.05.049>
- 36 Figueira, T.R., Melo, D.R., Vercesi, A.E. and Castilho, R.F. (2012) Safranin as a fluorescent probe for the evaluation of mitochondrial membrane potential in isolated organelles and permeabilized cells. *Methods Mol. Biol.* **810**, 103–117 https://doi.org/10.1007/978-1-61779-382-0_7
- 37 Laurindo, F.R., Fernandes, D.C. and Santos, C.X. (2008) Assessment of superoxide production and NADPH oxidase activity by HPLC analysis of dihydroethidium oxidation products. *Methods Enzymol.* **441**, 237–260 [https://doi.org/10.1016/S0076-6879\(08\)01213-5](https://doi.org/10.1016/S0076-6879(08)01213-5)
- 38 Zhou, R., Yazdi, A.S., Menu, P. and Tschopp, J. (2011) A role for mitochondria in NLRP3 inflammasome activation. *Nature* **469**, 221–225 <https://doi.org/10.1038/nature09663>
- 39 Bartz, R.R., Suliman, H.B. and Piantadosi, C.A. (2015) Redox mechanisms of cardiomyocyte mitochondrial protection. *Front. Physiol.* **6**, 291 <https://doi.org/10.3389/fphys.2015.00291>
- 40 Mekada, K., Abe, K., Murakami, A., Nakamura, S., Nakata, H., Moriwaki, K. et al. (2009) Genetic differences among C57BL/6 substrains. *Exp. Anim.* **58**, 141–149 <https://doi.org/10.1538/Expanim.58.141>
- 41 Attane, C., Peyot, M.L., Lussier, R., Zhang, D.W., Joly, E., Madiraju, S.R.M. et al. (2016) Differential insulin secretion of high-fat diet-fed C57BL/6NN and C57BL/6NJ mice: implications of mixed genetic background in metabolic studies. *PLoS ONE* **11**, e0159165 <https://doi.org/10.1371/journal.pone.0159165>
- 42 Fisher-Wellman, K.H., Ryan, T.E., Smith, C.D., Gilliam, L.A.A., Lin, C.T., Reese, L.R. et al. (2016) A direct comparison of metabolic responses to high-fat diet in C57BL/6J and C57BL/6NJ mice. *Diabetes* **65**, 3249–3261 <https://doi.org/10.2337/db16-0291>
- 43 Kim, A., Chen, C.H., Ursell, P. and Huang, T.T. (2010) Genetic modifier of mitochondrial superoxide dismutase-deficient mice delays heart failure and prolongs survival. *Mamm. Genome* **21**, 534–542 <https://doi.org/10.1007/s00335-010-9299-x>
- 44 Whitaker, R.M., Corum, D., Beeson, C.C. and Schnellmann, R.G. (2016) Mitochondrial biogenesis as a pharmacological target: a new approach to acute and chronic diseases. *Ann. Rev. Pharm. Toxic.* **56**, 229–249 <https://doi.org/10.1146/annurev-pharmtox-010715-103155>

- 45 Cherry, A.D. and Piantadosi, C.A. (2015) Regulation of mitochondrial biogenesis and its intersection with inflammatory responses. *Antioxid. Redox Signal.* **22**, 965–976 <https://doi.org/10.1089/ars.2014.6200>
- 46 Salminen, A., Ojala, J., Kaamiranta, K. and Kauppinen, A. (2012) Mitochondrial dysfunction and oxidative stress activate inflammasomes: impact on the aging process and age-related diseases. *Cell. Mol. Life Sci.* **69**, 2999–3013 <https://doi.org/10.1007/s00018-012-0962-0>
- 47 Hartman, J. and Frishman, W.H. (2014) Inflammation and atherosclerosis: a review of the role of interleukin-6 in the development of atherosclerosis and the potential for targeted drug therapy. *Cardiol. Rev.* **22**, 147–151 <https://doi.org/10.1097/CRD.0000000000000021>
- 48 Spears, L.D., Razani, B. and Semenkovich, C.F. (2013) Interleukins and atherosclerosis: a dysfunctional family grows. *Cell Metab.* **18**, 614–616 <https://doi.org/10.1016/j.cmet.2013.10.009>
- 49 Mungrue, I.N., Husain, M. and Stewart, D.J. (2002) The role of NOS in heart failure: lessons from murine genetic models. *Heart Fail. Rev.* **7**, 407–422 <https://doi.org/10.1023/a:1020762401408>
- 50 Green, S.J., Scheller, L.F., Marletta, M.A., Seguin, M.C., Klotz, F.W., Slayter, M. et al. (1994) Nitric oxide: cytokine-regulation of nitric oxide in host resistance to intracellular pathogens. *Immunol. Lett.* **43**, 87–94 [https://doi.org/10.1016/0165-2478\(94\)00158-8](https://doi.org/10.1016/0165-2478(94)00158-8)
- 51 Xia, Y. and Zweier, J.L. (1997) Superoxide and peroxynitrite generation from inducible nitric oxide synthase in macrophages. *Proc. Natl Acad. Sci. U.S.A.* **94**, 6954–6958 <https://doi.org/10.1073/pnas.94.13.6954>
- 52 Whitney, K.D., Watson, M.A., Goodwin, B., Galardi, C.M., Maglich, J.M., Wilson, J.G. et al. (2001) Liver X receptor (LXR) regulation of the LXRalpha gene in human macrophages. *J. Biol. Chem.* **276**, 43509–43515 <https://doi.org/10.1074/jbc.M106155200>
- 53 Alba, G., Reyes, M.E., Santamaria, C., Saenz, J., Ramirez, R., Geniz, I. et al. (2012) Transcription of liver X receptor is down-regulated by 15-deoxy-delta 12,14-prostaglandin J2 through oxidative stress in human neutrophils. *FEBS J.* **279**, 153–154 <https://doi.org/10.1371/journal.pone.0042195>
- 54 Yin, K., Liao, D.F. and Tang, C.K. (2010) ATP-binding membrane cassette transporter A1 (ABCA1): a possible link between inflammation and reverse cholesterol transport. *Mol. Med.* **16**, 438–449 <https://doi.org/10.2119/molmed.2010.00004>
- 55 McGillicuddy, F.C., de la Llera Moya, M., Hinkle, C.C., Joshi, M.R., Chiquoine, E.H., Billheimer, J.T. et al. (2009) Inflammation impairs reverse cholesterol transport in vivo. *Circulation* **119**, 1135–1145 <https://doi.org/10.1161/CIRCULATIONAHA.108.810721>
- 56 Yang, X.X., Yao, H., Chen, Y.L., Sun, L., Li, Y., Ma, X.Z. et al. (2015) Inhibition of glutathione production induces macrophage CD36 expression and enhances cellular-oxidized low density lipoprotein (oxLDL) uptake. *J. Biol. Chem.* **290**, 21788–21799 <https://doi.org/10.1074/jbc.M115.654582>
- 57 Vozenilek, A.E., Vetkoetter, M., Green, J.M., Shen, X., Traylor, J.G., Klein, R.L. et al. (2018) Absence of nicotinamide nucleotide transhydrogenase in C57BL/6J mice exacerbates experimental atherosclerosis. *J. Vasc. Res.* **55**, 98–110 <https://doi.org/10.1159/000486337>